Nano Research

Open Access

Review Article

Precisely constructing uniform polymeric nanomaterials

En Fang, Liangyu Chen, Zijun He, Weimin Wang, Junting Xu, and Shaofei Song ✉

MOE Key Laboratory of Macromolecular Synthesis and Functionalization, Department of Polymer Science and Engineering, Zhejiang University, Hangzhou 310027, China

Cite this article: *Nano Research*, **2026**, *19*, 94909021. https://doi.org/10.26599/NR.2026.94909021

ABSTRACT: Polymeric nanomaterials offer broad applicability in drug delivery, biomedicine, and functional materials due to their tunable size, morphology, and surface properties. However, achieving true uniformity—consistent size in all three dimensions, uniform morphology, and ordered internal packing—remains a central challenge. This review focuses on bottom-up strategies for constructing uniform polymeric nanomaterials, with particular emphasis on crystallization-driven self-assembly (CDSA). While living CDSA enables exceptional control over nanostructure length and lateral area along epitaxial growth directions (*a*/*b* axes), the independent regulation of dimensions in the non-growth direction (*c*-axis)—i.e., the diameter of one-dimensional (1D) fibers and the thickness of two-dimensional (2D) platelets—remains largely unmet due to the complexity of polymer chain folding. Unlike previous reviews that focus primarily on CDSA's morphological control, this review places the non-growth direction at the center of the design paradigm. We analyze why *c*-axis control is fundamentally harder, survey emerging molecular strategies, and present our own complementary approaches—controlled main-chain folding via precision defects and side-chain extended crystallization—that enable programmable thickness control. This review provides a mechanism-oriented framework for the precise, full-dimensional construction of uniform polymeric nanomaterials.

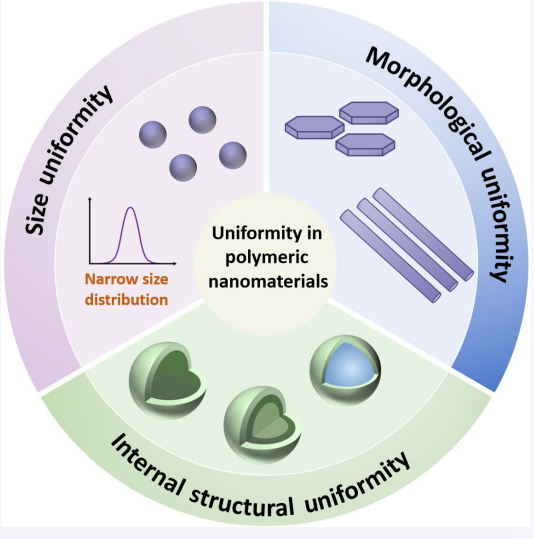

KEYWORDS: polymeric nanomaterials, uniformity, chain folding, crystallization-driven self-assembly, full-size control

1 Introduction

Polymeric nanomaterials are highly valuable in fields such as drug delivery, biomedicine, and functional materials due to the ability to tailor their size, morphology, surface properties, and internal structure [1–8]. However, for a long time, the self-assembly research has primarily focused on whether nanostructures can be obtained and what morphologies they can form. With significant advances in recent years, particularly in methods like crystallization-driven self-assembly (CDSA) [9–15], researchers have achieved remarkable control over the length of one-dimensional (1D) nanofibers and the lateral area of two-dimensional (2D) platelet micelles [16–36]. This undoubtedly represents a major step forward.

Received: June 12, 2026; **Revised:** July 10, 2026
Accepted: July 13, 2026

✉Address correspondence to songsf@zju.edu.cn

Nevertheless, for "uniform" polymeric nanomaterials, the definition should not be limited to size monodispersity in a single dimension [37]. As illustrated in Fig. 1, an ideal, highly uniform nanomaterial should exhibit three interconnected levels of uniformity: unified size in all three dimensions, consistent morphology across the population, and structural homogeneity (i.e., ordered chain packing) within each individual object. Unfortunately, most current strategies are focused on the direction of epitaxial crystal growth (the *a*/*b* axes) [38–42]. Controlling dimensions along the non-growth direction (the *c*-axis, corresponding to the diameter of 1D structures and the thickness of 2D platelets) remains a formidable and largely unmet challenge. Consequently, many reported "uniform" nanomaterials still suffer from an unacceptable distribution in thickness or diameter [41, 42].

The inability to control the non-growth direction stems from the fundamental complexity of polymer chain folding [43–52]. Unlike epitaxial growth, where size can be tuned predictably by adjusting seed numbers or unimer-to-seed ratios, chain folding is governed by a complex interplay of thermodynamic and kinetic factors,

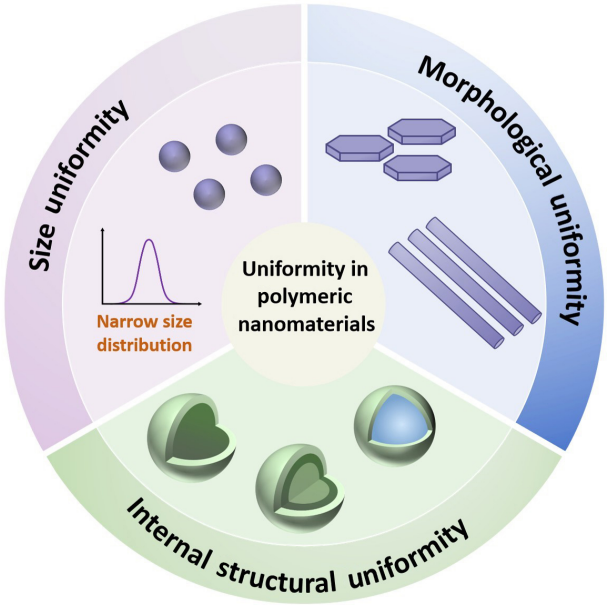

Figure 1 Overview of uniformity and construction of polymeric nanomaterials. Three levels of uniformity: size, morphology, and internal structure.

including molecular structure, crystallization temperature, and solvent conditions [44]. It has remained notoriously difficult to control precisely. Therefore, learning how to program polymer chain folding at the molecular design stage to enable predictable control over the thickness or diameter of crystalline nanomaterials is a critical and urgent scientific problem in polymer science and nanotechnology.

Unlike previous reviews that primarily focus on CDSA's morphological control and applications [14, 19, 22, 23, 33, 53–55], this review addresses a more advanced and challenging topic: How to achieve true three-dimensional (3D) precision in polymeric nanomaterials by controlling the non-growth direction through molecular design. We systematically analyze the limitations of current strategies, highlight recent progresses in controlling crystal thickness via main-chain folding and side-chain crystallization, and provide a new conceptual framework for moving from empirical size control toward truly programmable, 3D-precision design.

2 Overview of construction strategies for polymeric nanomaterials

Methods for constructing polymeric nanomaterials can be broadly categorized into "top-down" and "bottom-up" approaches. "Top-down" strategies fabricate nanoscale structures from bulk materials via processes like lithography, templating, or mechanical milling (Fig. 2) [56–61]. While indispensable for microelectronics, these methods often suffer from low throughput, high cost, and limited control over 3D uniformity and internal structure. For example, lithographically defined polymer dots often exhibit rough edges and amorphous internal packing, limiting their performance in optoelectronic devices [62]. For the purpose of this review, we primarily focus on "bottom-up" strategies, which build nanostructures from molecular or macromolecular building blocks [1–8, 63–69], as they offer superior potential for achieving precise, predictable, and complex architectures.

As illustrated in Fig. 3, bottom-up strategies can be further divided based on whether nanostructure formation is coupled with polymer chain growth.

The first route proceeds from monomers to nanomaterials directly. Polymerization-induced self-assembly (PISA) is a prime example [70–85]. Here, the growing polymer chain becomes insoluble in the reaction medium, triggering *in situ* self-assembly. PISA is highly efficient and can produce high concentrations of nano-objects like spheres, worms, and vesicles [73, 78]. However, because nucleation, growth, and morphology evolution are kinetically coupled, achieving narrow dispersity in size and precise control over complex morphologies, especially anisotropic ones like uniform fibers and platelets, remains challenging. Bottlebrush

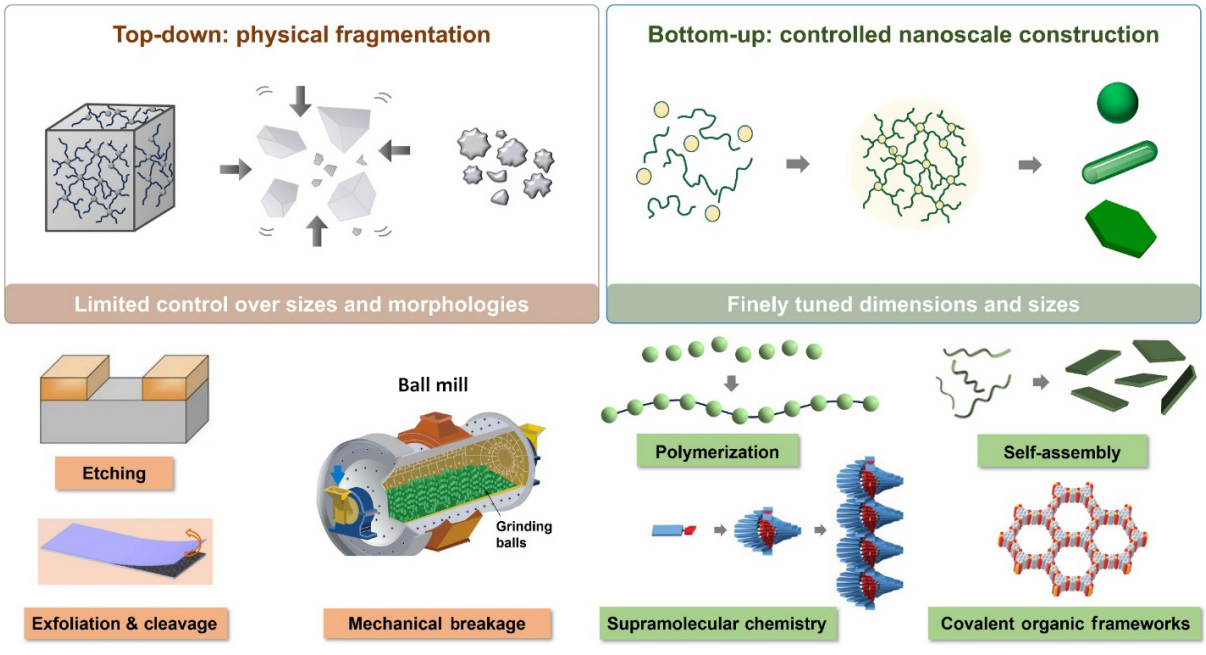

Figure 2 Uniformity and construction strategies of inorganic/organic nanomaterials. Schematic comparison of top-down and bottom-up strategies. Reproduced with permission from Ref. [63], © Macmillan Publishers Limited 2012; Ref. [64], © American Association for the Advancement of Science 2005.

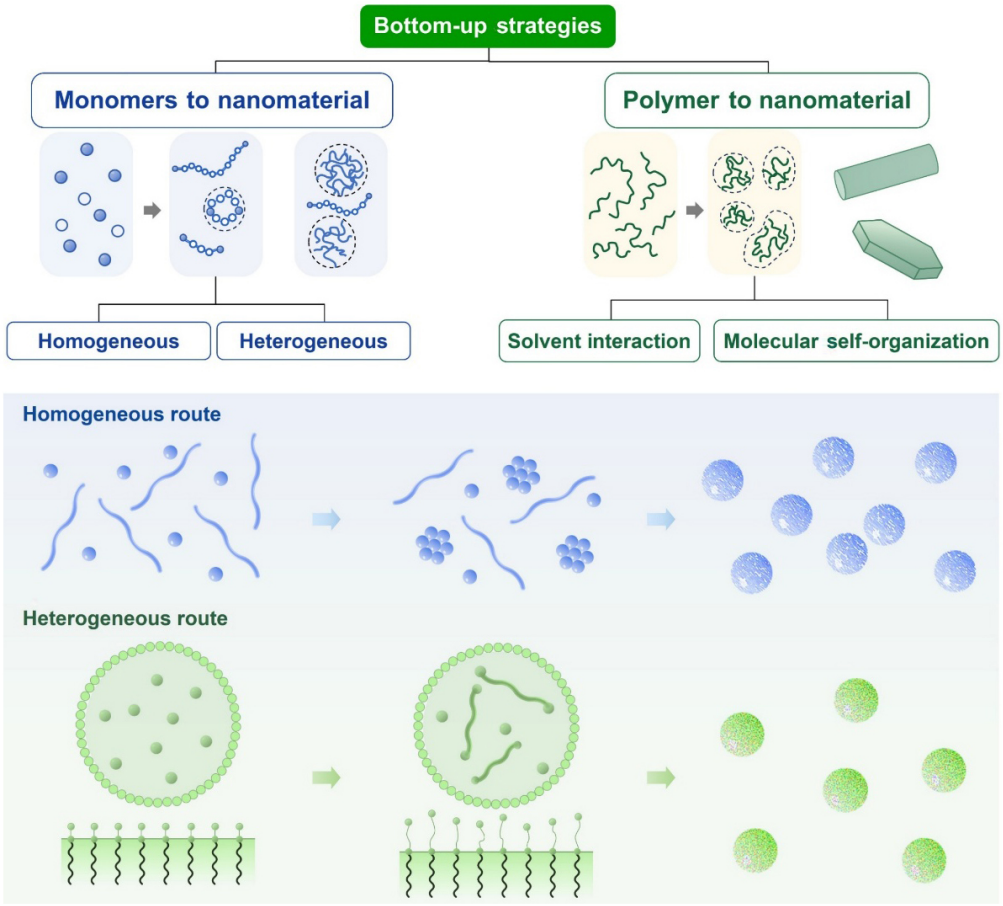

Figure 3 Polymer chemistry- or polymer physical chemistry-based formation routes. Bottom-up strategies are divided into polymerization-based formation (from monomers to nanomaterial) and preformed-polymer assembly route (from polymer to nanomaterial). Homogeneous routes are governed by phase separation and nucleation, whereas heterogeneous routes rely on confined microdomains.

polymers [86–101], another example of this route, produce unimolecular cylindrical nanoparticles, but their size is limited by the molecular design and synthesis.

The second route proceeds from preformed polymers to nanomaterials. This approach decouples polymer synthesis from nanostructure formation, allowing for more rational design of the final assembly. Solvent-mediated methods, like nanoprecipitation, are versatile for making spherical carriers but lack the ability to create highly ordered, anisotropic structures. In contrast, CDSA stands out as a particularly powerful strategy [2, 14, 19, 23, 33]. By using the crystallization of a core-forming block as the primary driving force, CDSA readily generates low-curvature morphologies such as 1D fibers and 2D platelets. Its "living" nature, through seeded growth, allows for exceptional control over the length (1D) and area (2D) of these nanostructures, which is a major advantage over PISA. The main challenge for CDSA, however, is scalability, though significant efforts are underway to address this via polymerization-induced CDSA (PI-CDSA) [102–105].

In summary, PISA offers high efficiency for simple spherical or vesicular morphologies but struggles with precise size control for anisotropic structures. In contrast, CDSA, particularly the living seeded-growth method, provides superior control over the dimensions of low-curvature, crystalline nanoparticles along their growth direction, making it the method of choice for constructing uniform 1D and 2D materials, despite current scalability challenges.

3 From monomers to nanomaterials: polymerization-induced self-assembly and bottlebrush polymers

Having established the broad classification of bottom-up strategies into polymerization-based formation routes and preformed-polymer assembly routes, we now turn our attention to the first of these two categories: polymerization-based formation. In this approach, nanostructures are not assembled from pre-existing polymers but are generated *in situ* during the polymerization reaction itself. The key distinction here is that chain growth and nanostructure formation are coupled and co-evolve, offering a direct and often highly efficient pathway from small molecule monomers to complex nano-objects. Among the various methods within this category, two have emerged as particularly powerful and conceptually distinct: PISA and the synthesis of bottlebrush polymers. While both originate from monomers, they differ fundamentally in their formation mechanisms and in the nature of the resulting nanomaterials. The following section will critically examine these two strategies, highlighting their principles, capabilities, and inherent limitations in the context of constructing uniform polymeric nanostructures.

In the "bottom-up" construction of polymeric nanomaterials, a conceptually straightforward route is to couple the process of polymer chain growth directly with nanostructure formation. This "monomer-to-nanomaterial" strategy bypasses the need for pre-

synthesized polymers and their subsequent processing. Instead, it leverages the polymerization reaction itself to induce phase separation, chain ordering, or spatial confinement, leading to the *in situ* generation of nano-objects. Among the various methods in this category, PISA and the synthesis of bottlebrush polymers represent two distinct and powerful platforms. While both originate from monomers, they differ fundamentally in their structure–formation mechanisms, the nature of the resulting nano-objects, and the degree of control over size and morphology.

3.1 Polymerization-induced self-assembly

PISA has emerged as a highly efficient and versatile platform for producing concentrated dispersions of block copolymer nano-objects for a few years [70–85]. In a typical PISA formulation, a soluble macromolecular chain transfer agent (macro-CTA) or stabilizer block is first dissolved in a suitable solvent (the reaction medium). A second monomer, which forms a polymer that is insoluble in this medium, is then polymerized. As the second block grows, it reaches a critical chain length where it becomes solvophobic, triggering an *in situ* self-assembly process. This process is fundamentally a polymerization-induced phase separation, where the growing polymer chains simultaneously undergo chain extension and aggregation into well-defined core–shell nanoparticles (Figs. 4(a) and 4(b)).

The key advantage of PISA lies in its efficiency and scalability [73, 78]. It can be performed at high solid contents (often 10%–50% w/w) in a one-pot reaction, yielding spherical micelles, worm-like micelles, or vesicles, simply by controlling the degree of polymerization of the core-forming block and the overall block composition. For example, reversible addition/fragmentation chain transfer (RAFT)-mediated dispersion polymerization has been extensively used to construct detailed morphology phase diagrams, enabling relatively predictable transitions between spheres, worms, and vesicles [70]. This represents a significant advance over traditional post-polymerization self-assembly methods, which are typically performed at low concentrations and in multiple steps.

Despite its efficiency, PISA faces inherent challenges in achieving precise control over the dimensions of anisotropic nanostructures. While the transition between morphologies (e.g., from spheres to worms to vesicles) can be mapped, the precise length of worm-like micelles or the lateral dimensions of vesicles are difficult to tune independently and often exhibit broad dispersity. The formation and growth of these nanostructures are kinetically coupled; nucleation, growth, and morphological evolution occur concurrently, making it difficult to decouple these processes for precision control. Furthermore, the morphologies accessible via standard PISA are largely limited to high-curvature objects (spheres, worms, vesicles), and the formation of low-curvature, crystalline, anisotropic structures such as uniform 1D fibers or 2D platelets is not typically observed. Attempts to combine PISA with crystallization processes (PI-CDSA) have been made to access such structures [102–105], but precise dimensional control (e.g., fiber length) often requires a subsequent seeded-growth step, which adds complexity.

3.2 Bottlebrush polymers

Bottlebrush polymers are a distinct class of macromolecules characterized by polymeric side chains densely grafted onto a linear polymer backbone [86–101]. Their unique architecture, where the steric repulsion between densely packed side chains forces the backbone into an extended, worm-like conformation, makes them intriguing "unimolecular nanoparticles". Unlike PISA, where nano-objects are formed by the association of many polymer chains, a bottlebrush polymer is a single, covalent macromolecule that is itself a nanoscale object (Figs. 4(c) and 4(d)). This fundamental difference has profound implications for uniformity and control. Because a bottlebrush is a single molecule, its dimensions are not subject to the statistical distribution of an aggregation number; its length is determined by the degree of polymerization (DP) of the backbone, and its diameter is determined by the DP and size of the side chains (Fig. 4(e)).

The most powerful synthetic route to well-defined bottlebrush polymers is the "graft-through" approach using ring-opening metathesis polymerization (ROMP) of norbornene-terminated macromonomers (MMs) [86]. The highly active and functional-group-tolerant Grubbs' catalysts (e.g., G3) enable rapid and controlled polymerization of even bulky MMs, yielding bottlebrushes with high grafting density, predetermined molecular weight, and low dispersity.

Recent advances have dramatically expanded the architectural complexity accessible by this method. For example, Johnson and co-workers developed an elegant "ROMP-of-ROMP" strategy, where a norbornene-terminated polynorbornene imide (PNI) MM is first synthesized by ROMP [101]. This MM is then used as a building block for a second, "graft-through" ROMP to produce a new generation of bottlebrush polymers (Fig. 4(c)). This modular approach provides access to unprecedented hierarchical architectures, including brush-on-brush (BoB) polymers where both the backbone and the side chains are themselves bottlebrushes. Furthermore, by using branched MMs with two different polymer chains attached to a single norbornene, the same group has created Janus bottlebrush copolymers. In these polymers, two chemically distinct side chains (e.g., rigid PNI and flexible PDMS) are arranged in a pseudo-alternating fashion along the backbone.

The exceptional control over molecular architecture afforded by graft-through ROMP allows for a direct and predictable structure–property relationship. The extended backbone conformation arising from densely grafted side chains, especially when the side chains are rigid (e.g., PNI), leads to unusually large domain spacings in self-assembled bulk morphologies. Johnson's work showed that diblock bottlebrush copolymers could form lamellae with a domain spacing close to the fully extended backbone length, a result that is not typical for coil-like block copolymers. Moreover, the Janus architecture, combined with side chain rigidity, can shift the phase boundary, stabilizing asymmetric lamellar morphologies even at volume fractions where cylindrical phases would be expected. This level of control over both molecular and nanoscale dimensions is a hallmark of the bottlebrush platform.

In summary, PISA is an exceptionally scalable and efficient method for creating concentrated, morphologically diverse (spheres, worms, vesicles) nano-objects from monomers. Its primary limitation lies in the difficulty of achieving precise, independent control over the dimensions of anisotropic structures. Conversely, the graft-through ROMP of MMs provides a uniquely powerful platform for constructing unimolecular bottlebrush nanoparticles with unprecedented precision over their molecular dimensions. While bottlebrushes are inherently 1D cylindrical objects, they can serve as highly controlled building blocks for creating more complex, hierarchical assemblies with predictable

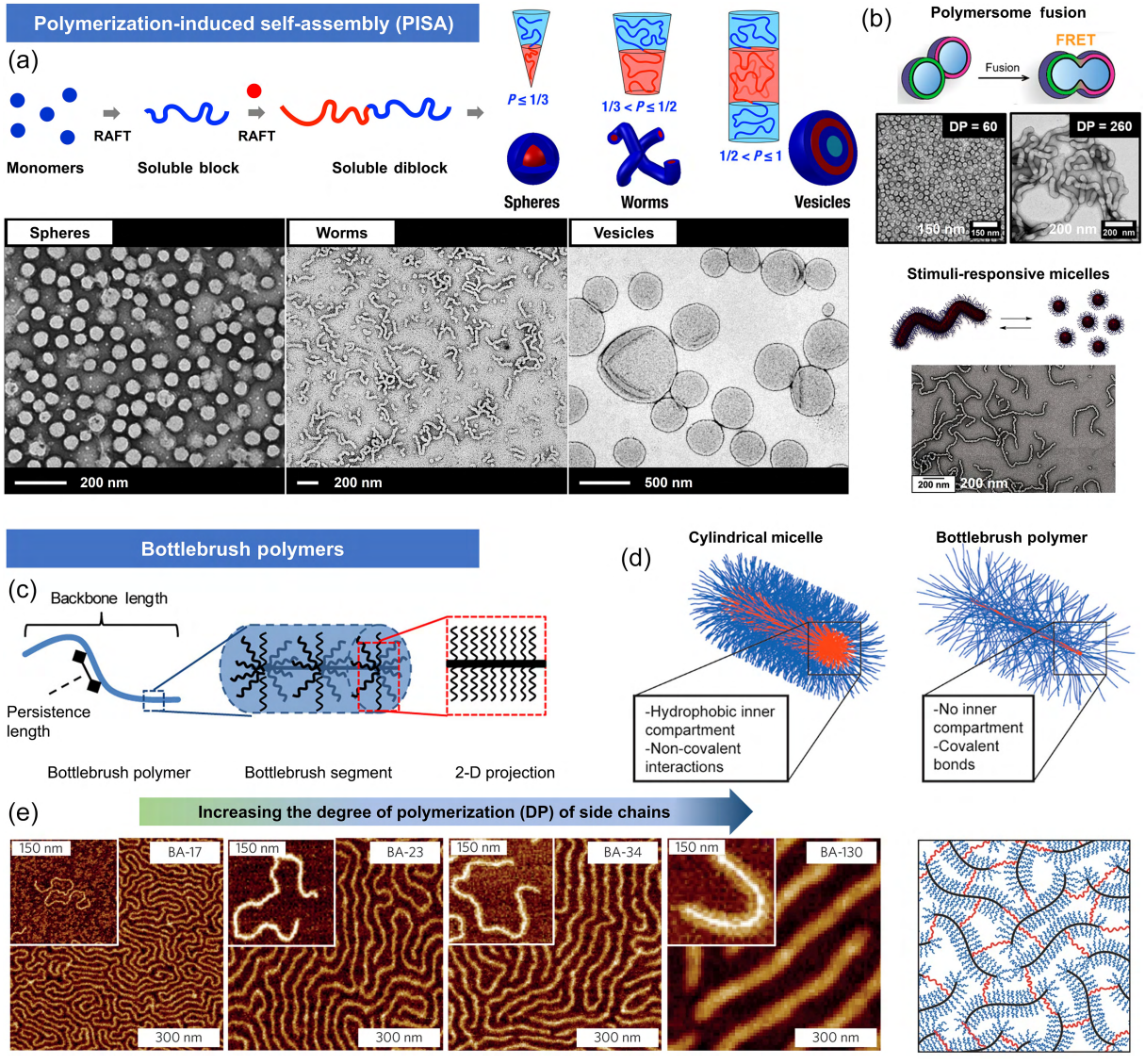

Figure 4 From monomers to nanomaterial by *in situ* polymerization such as PISA and synthesis of bottlebrush polymers. (a) Representative three kinds of morphologies of nanomaterials by PISA. Reproduced with permission from Ref. [70], © American Chemical Society 2016. (b) Polymersome fusion and external stimuli can produce new morphologies. Reproduced with permission from Ref. [91], © American Chemical Society 2019. (c) Scheme of bottlebrush polymers. Reproduced with permission from Ref. [72], © American Chemical Society 2013. (d) There are differences between cylindrical micelle and bottlebrush polymer. Reproduced with permission from Ref. [75], © Mitchell, D. E. et al. 2016; Ref. [90], © American Chemical Society 2019. (e) The length and width of bottlebrush polymer can be controlled by the degrees of polymerization (DPs) of main chain and side chain respectively. Reproduced with permission from Ref. [88], © WILEY-VCH Verlag GmbH & Co. KGaA, Weinheim 2015; Ref. [89], © Macmillan Publishers Limited 2016.

domain spacings. The choice between these two strategies depends on the target application: PISA for high-volume, morphologically simple carriers, and bottlebrush polymers for precision nanomaterials where size, shape, and function are defined at the molecular level.

4 Preformed-polymer assembly: From traditional self-assembly to crystallization-driven self-assembly

4.1 Traditional self-assembly: Driving forces and limitations

Before discussing crystallization-driven self-assembly, it is instructive to briefly consider traditional self-assembly. Traditional self-assembly refers to polymer self-organization processes that are not dominated by crystal growth, but instead driven by segmental incompatibility, solvophobic effects, or specific intermolecular interactions[1–8]. Extensive studies on block copolymer self-assembly have shown that polymer chain composition, block volume fraction, solvent selectivity, and segmental interactions jointly influence the final assembled morphology, including spherical micelles, worm-like micelles, vesicles, and more complex hierarchical or multicompartment aggregates [8].

In selective solvents, insoluble blocks aggregate to form solvophobic cores, while soluble blocks extend outward to form coronas that provide colloidal stabilization. The morphological evolution of these aggregates can be qualitatively analyzed using the packing parameter (Fig. 4(a)) [70], $p = v/(a_0 l_c)$, where v is the

volume of the hydrophobic block, a_0 is the effective area of the hydrophilic head group, and l_c is the critical chain length. Higher curvature favors spherical micelles ($p \leq 1/3$), intermediate curvature corresponds to worm-like or rod-like micelles ($1/3 < p \leq 1/2$), and lower curvature favors vesicles or lamellae ($p > 1/2$). However, for polymeric systems, the packing parameter cannot be treated as the sole determining factor. Polymer composition, solvent selectivity, concentration, temperature, and the pathway of solvent change all affect the final morphology. Moreover, polymer self-assembled structures often do not correspond strictly to thermodynamic equilibrium states; their final morphology and uniformity are influenced by chain-exchange dynamics, preparation history, and structural rearrangement kinetics.

In addition to solvophobic effects, specific intermolecular interactions—such as electrostatic complexation, hydrogen bonding, metal coordination, and π–π stacking—can also drive the formation of stable or functionalized nanostructures [1–8]. While these interaction-driven assemblies offer rich opportunities for stimuli-responsive and functional materials, their structural uniformity and stability depend sensitively on precise regulation of composition, interaction strength, and solution environment.

Despite the remarkable progress in traditional self-assembly, several inherent limitations persist [7, 8]. First, the accessible morphologies are predominantly high-curvature structures (spheres, worms, vesicles), and the formation of low-curvature, anisotropic architectures such as uniform 1D fibers and 2D platelets remains challenging. Second, the dimensions of the resulting assemblies are difficult to predict and control independently, as they are governed by a complex interplay of thermodynamic and kinetic factors. Third, the dynamic nature of these assemblies (e.g., chain exchange) can lead to structural evolution over time, compromising long-term uniformity. These limitations have motivated the search for alternative driving forces that can confer greater predictability and directional control over nanostructure formation.

4.2 Polymer crystallization: A powerful driving force for anisotropic assembly

In stark contrast to the solvophobicity-driven processes described above, harnessing polymer crystallization as a driving force for self-assembly offers a powerful route to ordered, anisotropic nanostructures. Polymer crystallization is a fundamental phase transition in which flexible polymer chains overcome conformational entropy to adopt ordered, periodic arrangements. Unlike small molecules that typically crystallize completely, polymers are inherently semicrystalline, forming hierarchical structures composed of ordered crystalline lamellae embedded in an amorphous matrix. The primary origin of this lamellar morphology is chain folding: A single polymer chain repeatedly folds back and forth upon itself to form a crystalline platelet, the thickness of which is typically on the order of 5–20 nm. Figures 5(a)–5(c) illustrate chain folding—the molecular process that ultimately determines *c*-axis thickness [44, 106, 107].

The classical understanding of polymer crystallization, largely developed from studies on polyethylene and isotactic polypropylene, posits that chain folding is dictated by a delicate interplay of thermodynamic driving force (undercooling) and kinetic barriers [106]. The resulting lamellar thickness is not fixed but is determined by crystallization conditions, particularly temperature. Higher crystallization temperatures (lower undercooling) favor thicker, more perfect lamellae, while rapid cooling leads to thinner, kinetically trapped lamellae. This sensitivity to processing conditions has historically made it difficult to predict and precisely control crystal dimensions from molecular structure alone.

Recent advances, however, have begun to challenge this purely processing-centric view. Studies on precision polymers have demonstrated that the regular incorporation of defects—such as alkyl branches, polar groups, or cyclic units—can profoundly influence crystallization behavior [108–113]. When the defect size is sufficiently large to be excluded from the crystalline lattice, the crystallizable segments are forced to fold at the defect sites, leading to lamellar thickness that correlates with the spacing between defects. This concept of chain folding by design represents a paradigm shift: from viewing chain folding as an uncontrollable kinetic outcome to treating it as a structural parameter that can be programmed by primary chain architecture. Furthermore, certain atactic polymers can crystallize when strong intermolecular forces (e.g., hydrogen bonding in poly(vinyl alcohol) or dipolar interactions in polyacrylonitrile) overcome configurational disorder. 106 polymers containing cyclic units (e.g., cyclopentane) have also been shown to exhibit "tacticity-independent" crystallization, where conformational flexibility allows ordered packing despite random stereochemistry. These insights have collectively expanded the toolkit for designing crystallizable polymer systems suitable for self-assembly.

4.3 Crystallization-driven self-assembly: Principles and mechanisms

The transition from understanding polymer crystallization to utilizing it as a tool for solution-phase self-assembly of block copolymers defines the field of CDSA (Figs. 5(d)–5(f)). In a typical CDSA experiment, a block copolymer containing a crystallizable core-forming block (e.g., polyferrocenylsilane (PFS); polylactide (PLA); polycaprolactone (PCL); or poly(3-hexylthiophene) (P3HT)) and a soluble corona-forming block is dissolved in a good solvent for both blocks. Upon the addition of a selective solvent (a non-solvent for the core block) or upon cooling, the core block undergoes crystallization [14–23]. This crystallization event provides an additional, powerful free-energy driving force that fundamentally alters the self-assembly landscape compared to traditional amphiphilic assembly.

Unlike conventional block copolymer micellization, where spherical micelles are the most common morphology, CDSA strongly favors low-curvature, anisotropic structures, such as 1D cylindrical (fiber-like) micelles and 2D platelet micelles [9–27, 114]. This preference arises because the formation of a crystalline core imposes a high energetic penalty for curvature; the system minimizes this penalty by forming flat or gently curved crystalline lamellae. Consequently, CDSA offers a direct and predictable route to anisotropic nanoparticles that are difficult to access via traditional self-assembly.

The mechanism of CDSA is best understood as a two-step process: nucleation and growth. Initially, a small number of crystalline nuclei form spontaneously (homogeneous nucleation). Once formed, these nuclei can act as seeds for the epitaxial crystallization of further unimers. This seeded growth mechanism is the key to achieving size control. If the number of seeds is fixed, the final length (for 1D fibers) or area (for 2D platelets) of the nanostructures becomes directly proportional to the amount of unimer added. This "living" characteristic of CDSA, first

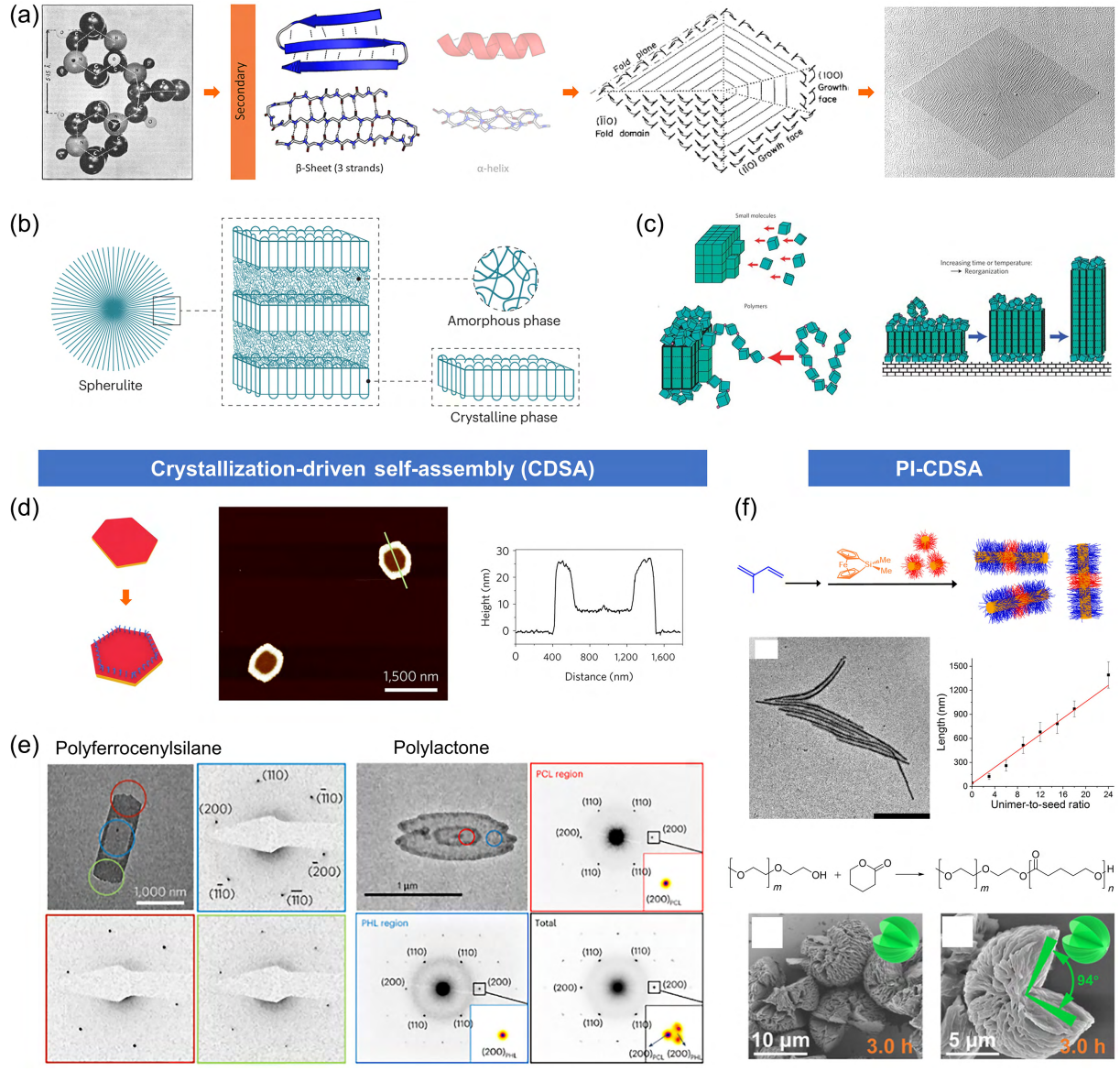

Figure 5 From polymers to nanomaterial via polymer crystallization and crystallization-driven self-assembly. (a) Chain folding to form the crystals. Reproduced with permission from Ref. [44], © Elsevier B.V. 2018. (b) Chain packing in the typical polymer crystal i.e. spherulite. Reproduced with permission from Ref. [106], © Springer Nature Limited 2026. (c) Illustration of the transition from chain-folding crystallization to annealing-induced thickening in self-seeding growth of polymer single crystals. Reproduced with permission from Ref. [107], © Macmillan Publishers Limited. (d) Seeded growth to form platelet block morphologies and the height/thickness of crystals. Reproduced with permission from Ref. [114], © Macmillan Publishers Limited, part of Springer Nature 2017. (e) ED pattern offering crystallographic information. Reproduced with permission from Ref. [27], © Tong, Z. Z. et al. 2023. (f) PI-CDSA to access uniform crystals. Reproduced with permission from Ref. [103], © American Chemical Society 2018; Ref. [105], © American Chemical Society 2026.

demonstrated by Manners and Winnik for PFS-based block copolymers [9, 14], is the cornerstone of modern precision nanomaterial synthesis using this method. The crucial distinction from traditional self-assembly and solvent-mediated particle formation is that uniformity and dimensional control in CDSA are not derived from narrow droplet size distributions or rapid mixing, but from the controlled, directional process of epitaxial crystallization on pre-formed, crystalline seeds [12–23]. This allows for the decoupling of nucleation from growth, enabling unprecedented predictability over nanostructure dimensions.

In summary, while traditional self-assembly offers flexibility in generating diverse soft-matter nanostructures, it struggles with predictive control over dimensions and the formation of low-curvature, anisotropic morphologies. CDSA, by harnessing the directional and cooperative nature of polymer crystallization, overcomes these limitations, providing a robust platform for constructing uniform 1D and 2D nanostructures with predictable dimensions. The following sections will discuss in detail the use of CDSA for preparing low-dimensional (Section 5.1) and three-dimensional (Section 5.2) nanomaterials.

5 Controlled construction of low-dimensional and three-dimensional nanomaterials via CDSA

CDSA has established itself as a uniquely powerful bottom-up strategy for constructing uniform polymeric nanomaterials, particularly those with low-curvature anisotropic morphologies that are difficult to access via traditional solvophobic-effect-driven

assembly. By introducing crystallization of a core-forming block as an additional free-energy driving force, CDSA fundamentally alters the self-assembly landscape. The crystalline core imposes a high energetic penalty for curvature, thereby favoring the formation of 1D cylindrical fibers, 2D platelets, and even complex 3D architectures [115–117]. Unlike conventional self-assembly, where spherical micelles dominate, CDSA provides a predictable route to anisotropic nanostructures with enhanced internal order.

5.1 Low-dimensional nanomaterials (1D and 2D): Morphology control and size regulation

The preparation of low-dimensional nanomaterials via CDSA can be broadly divided into direct CDSA and living CDSA, which differ fundamentally in their nucleation and growth pathways.

Direct CDSA refers to the formation of crystalline-core nanostructures by directly inducing crystallization nucleation and growth through changes in temperature or solvent quality from an initial single-chain or weakly aggregated state [14]. Thermally induced CDSA typically involves first heating the polymer to melt or fully dissolve crystallizable blocks, thereby erasing thermal history and residual aggregates, followed by controlled cooling to trigger nucleation and growth. Solvent-switch-induced CDSA involves dissolving the polymer in a good solvent and then introducing a selective or poor solvent to reduce solubility of the crystallizable block, driving aggregation and crystallization. While direct CDSA is operationally simple and effective for illustrating fundamental crystallization-driven formation mechanisms, it suffers from a critical limitation: Nucleation and growth are not decoupled. Nuclei form at different times and continue growing under different residual unimer concentrations, leading to broad distributions in fiber length or platelet except in very few cases [20, 21]. Therefore, direct CDSA alone is insufficient for applications requiring high size uniformity area.

To overcome this limitation, living CDSA strategies have been developed, which separate nucleation from subsequent growth by using pre-formed or selectively retained crystalline seeds as starting points for epitaxial crystallization. Two primary living CDSA strategies are widely employed: seeded growth [12] and self-seeding [13, 107].

Seeded growth is the most representative living CDSA strategy. In this approach, 1D fibers or 2D platelets are first prepared by direct CDSA, then fragmented by ultrasonication or shearing to generate relatively uniform crystalline seeds that retain ordered lattices. When unimers are added to a seed suspension under conditions that suppress spontaneous nucleation, epitaxial crystallization occurs preferentially at the seed ends (for 1D fibers) or crystal faces (for 2D platelets). The final length of 1D fibers or the lateral area of 2D platelets becomes directly proportional to the unimer-to-seed mass ratio, provided the seed number is fixed and new nucleation is effectively suppressed. This "living" characteristic enables predictable, quantitative control over nanostructure dimensions along the epitaxial growth direction (*a*/*b* axes) [12, 118, 119]. Moreover, seeded growth can be extended to heteroepitaxial growth by sequentially adding unimers with different compositions or corona structures, yielding segmented, patchy, or hierarchical block comicelles. For example, 1D block comicelles with spatially distinct coronas can be constructed by sequential addition of different block copolymers [119]. Similarly, 2D patchy platelets with controlled compositional patterns have been achieved via seeded heteroepitaxial growth in two dimensions [120]. These capabilities position seeded growth as a powerful methodology not only for size regulation but also for constructing spatially defined, multicomponent crystalline nanostructures.

Self-seeding offers an alternative living CDSA strategy that does not require externally added seeds [13, 107]. Instead, endogenous crystal fragments are selectively retained within the original crystalline nanostructures through partial melting or partial dissolution. Upon subsequent cooling or solvent-quality change, released unimers epitaxially grow on the surfaces of these residual crystals, thereby improving size distribution. Self-seeding is procedurally simpler than seeded growth because it eliminates the need for separate seed preparation [121]. However, its size control is more sensitive to processing conditions, including annealing temperature, solvent composition, and the stability of residual crystalline fragments [122]. The number of endogenous seeds is determined indirectly by thermal or solvent treatment, rather than being preset by the experimenter. Consequently, while self-seeding can effectively narrow size distributions, it does not offer the same level of predictable, independent dimensional control as seeded growth, where dimensions are directly set by the unimer-to-seed ratio.

Together, these living CDSA strategies have enabled the preparation of uniform 1D fibers and 2D platelets with precisely controlled lengths and lateral areas, as summarized schematically in Figs. 6(a)–6(c) [41, 42, 117, 118, 123, 124]. The figure illustrates how seeded growth and self-seeding decouple nucleation from subsequent epitaxial growth, allowing improved control over dimensions and dispersity for 1D cylinders, 2D platelets, and hybrid 1D/2D structures.

5.2 Three-dimensional nanomaterials: From branched structures to spherulites

Building upon the success of living CDSA for 1D and 2D nanomaterials, researchers have increasingly turned their attention to constructing 3D polymeric nanostructures (Fig. 7). The figure pairs schematic representations with corresponding TEM, SEM, or optical microscopy images, illustrating branched structures, sheaf-like aggregates, hedrites, and mature spherulites. These 3D architectures—including branched micelles, flower-like structures, sheaf-like aggregates, hedrites, and uniform spherulites—represent a higher level of morphological complexity that is both biologically inspired and technologically relevant [21, 115, 116, 125–131].

Branched structures are among the most frequently reported 3D morphologies in CDSA. They can be generated through several distinct strategies. Multistep seeded growth allows the sequential addition of different unimers to seed crystals, leading to fiber-like tassels protruding from platelet ends, forming scarf-like or multiarmed structures. Homopolymer/block copolymer blends provide another route: Homopolymer nanocrystals can serve as multi-active initiation sites, nucleating fiber growth from multiple directions to form star-like branched micelles [117, 125]. The cooling rate during assembly is also critical; rapid cooling increases supersaturation, promoting seed aggregation and the formation of multiple active growth sites, thereby favoring branched over linear morphologies [122]. Corona chain modification represents yet another powerful strategy. Partial removal or chemical modification of corona chains—such as photocleavage, quaternization, or introduction of amino groups—reduces corona repulsion, allowing unimers to attach not only at termini but also along lateral faces, leading to branched architectures. Solvent composition further modulates branching behavior: Swelling the crystalline core with a good solvent reduces corona repulsion and promotes lateral growth

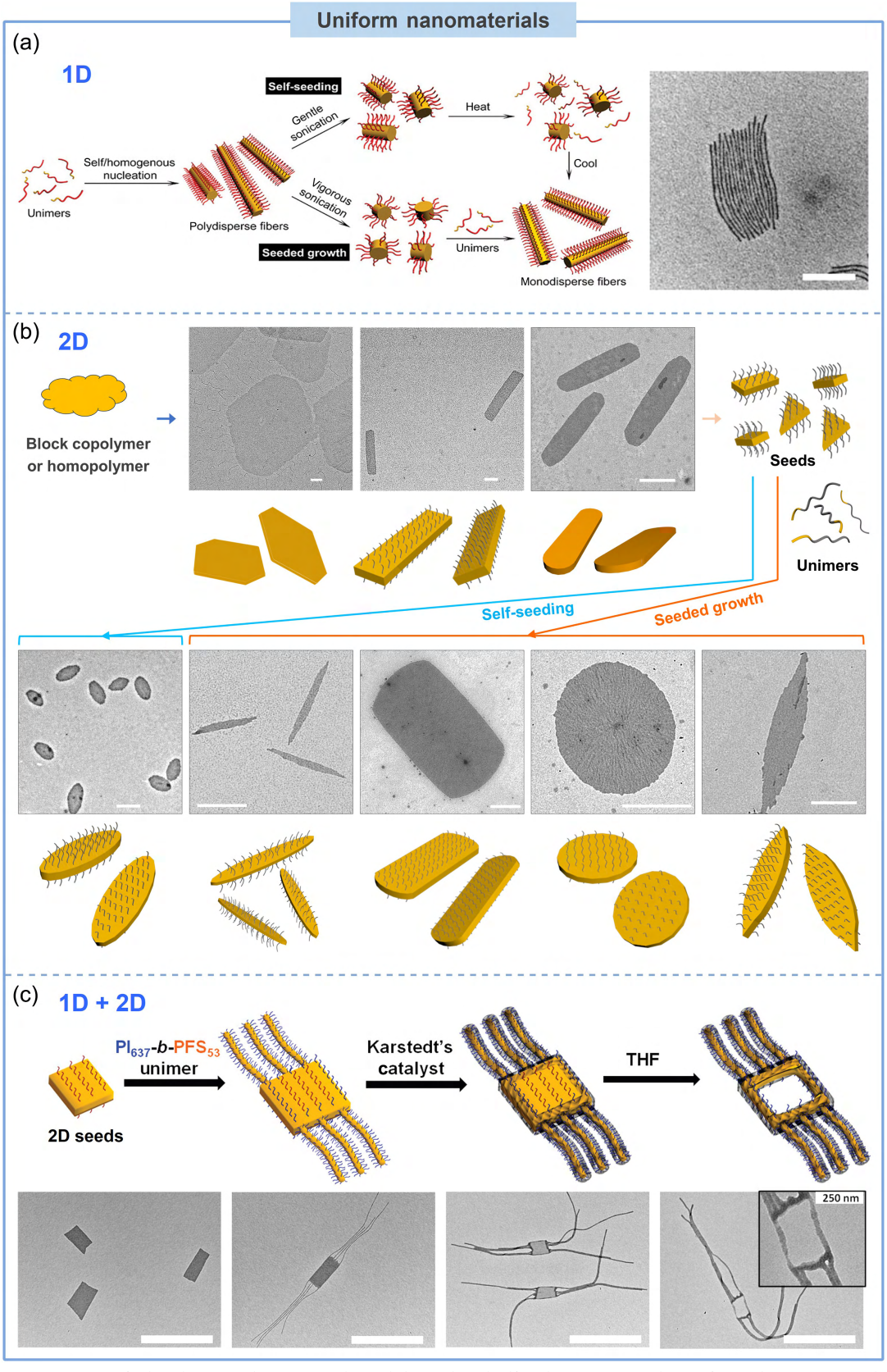

Figure 6 Living CDSA strategies for low-dimensional nanomaterials. Seeded growth and self-seeding separate nucleation from subsequent epitaxial growth, enabling improved control over the dimensions and dispersity of crystalline polymer nanostructures, (a) 1D cylinders, (b) 2D platelets, and (c) hybrid 1D/2D structure. Scale bars of TEM images, (a) 500 nm; (b) 1000 nm; (c) 2000 nm. Reproduced with permission from Ref. [41], © The Royal Society of Chemistry 2020; Ref. [42], © American Chemical Society 2021; Ref. [117], © American Chemical Society 2015; Ref. [118], © Macmillan Publishers Limited 2010; Ref. [123], © American Chemical Society 2026; Ref. [124], © Macmillan Publishers Limited 2009.

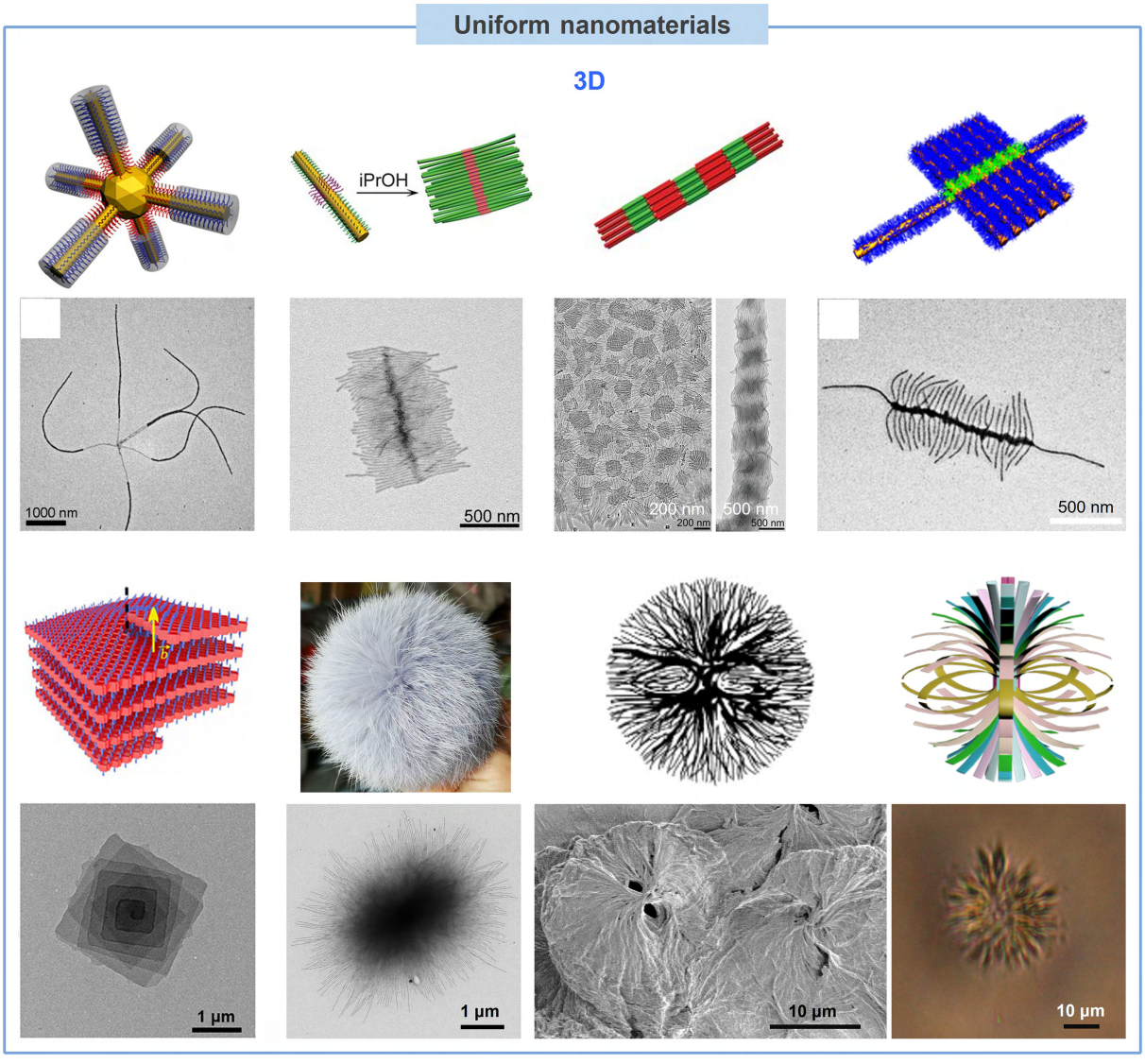

Figure 7 Living CDSA strategies for 3D nanomaterials. By seeded growth or self-seeding, 3D polymeric nanostructures or biomimetic nano-morphologies can be accessed. The objects in the first and third rows are schemes of the assemblies in second and fourth rows acquired by TEM/SEM/OM images. Reproduced with permission from Ref. [21], © Elsevier Inc. 2021; Ref. [115], © Wiley-VCH GmbH 2021; Ref. [125], © American Chemical Society 2013; Ref. [127], © American Association for the Advancement of Science 2015; Ref. [129], © American Chemical Society 2016; Ref. [130], © American Chemical Society 2020.

into ribbon precursors, which subsequently evolve into complex biomorphic branched structures [132].

Beyond simple branched morphologies, CDSA has enabled the formation of more sophisticated 3D assemblies. Flower-like structures, for instance, have been observed in triblock copolymers where a terminal fluorescent block exhibits limited solubility, causing cylindrical micelles to aggregate into flower-like objects [133]. More remarkably, recent advances have demonstrated the formation of uniform polymer spherulites in dilute solution, a phenomenon previously known only in bulk polymer melts, geology, and biology but unprecedented in block copolymer solution self-assembly [115]. Spherulites are spherically symmetric crystal colonies that evolve through distinct intermediate stages: from uniform oval platelets to lenticular forms, then to hedrites, sheaf-like micelles, and finally to mature spherulites with characteristic "two eyes" morphology (Fig. 7). The key to accessing these 3D structures lies in achieving high supersaturation and controlled secondary crystallization. Under appropriate conditions such as specific corona/core block ratios (typically between 1 and 5.5), careful annealing temperatures, and controlled cooling, defects initially form in lamellar precursors. These defects act as nucleation sites for secondary crystals on basal faces, followed by non-crystallographic branching and lamellar twisting driven by anisotropic surface stresses. The "living" nature of CDSA is particularly valuable for studying spherulite formation because growth stops upon unimer exhaustion, allowing intermediates to be isolated and characterized.

General protocols for generating uniform spherulites and their precursors have now been extended to various PFS-based block copolymer systems in both polar and nonpolar solvents, suggesting a broader applicability. Key prerequisites include corona/core block ratios that favor initial 2D structure formation and subsequent secondary crystallization. Importantly, the transition from 2D to 3D morphologies is driven by increasing supersaturation and defect engineering, rather than by simple epitaxial growth along a single direction [116].

In summary, CDSA offers a robust and versatile platform for constructing uniform low-dimensional and three-dimensional polymeric nanomaterials. Living CDSA strategies—particularly seeded growth—enable predictable control over dimensions along epitaxial growth directions for 1D fibers and 2D platelets. Extensions of these methods to 3D architectures, including branched structures, flower-like assemblies, and uniform spherulites, have opened new avenues for biomimetic and functional nanomaterials. Nevertheless, achieving full three-dimensional control—including thickness and diameter—remains an outstanding challenge that will require molecular-level design strategies to program chain folding and crystal packing.

6 Current problems in CDSA: The challenge of controlling non-growth-direction dimensions

Over the past two decades, living CDSA has emerged as a powerful strategy for constructing uniform polymeric nanomaterials. Through seeded growth and self-seeding protocols, researchers have achieved remarkable control over the length of 1D fibers and the lateral area of 2D platelets. However, a critical challenge remains: the inability to independently control dimensions in the *c*-axis (non-growth direction). This section focuses on the consequences of this limitation and why solving it matters for real-world applications.

Figure 8 presents direct evidence of this challenge which show single crystals (Figs. 8(a) and 8(b)) where lateral dimensions are well-defined but thickness remains unregulated. Figure 8(c) defines the *a*/*b* (growth) and *c* (non-growth) axes [134]. As shown in Fig. 8(d), atomic force microscopy (AFM) height profiles directly reveal the distribution in platelet thickness, underscoring the lack of *c*-axis control—even when lateral dimensions are highly uniform. This problem is not merely academic. The thickness dimension, though only a few nanometers, profoundly influences key material properties and device performance. In organic optoelectronics and semiconductor applications, for example, charge carrier mobility and exciton diffusion efficiency are highly sensitive to the out-of-plane (*c*-axis) dimension of 2D polymer crystals [135]. In membrane technologies, thickness directly dictates selectivity and permeance. A variation of ±1 nm in lamellar thickness can alter the electronic coupling between adjacent layers by more than an order of magnitude, leading to inconsistent device performance. 135 As modern technology pushes toward ever-smaller length scales, the demand for truly three-dimensional precision in polymer nanomaterials has become urgent.

The post-Moore era of semiconductor chip manufacturing provides a compelling illustration. The industry is shifting from traditional 2D planar integration toward 3D monolithic integration [136, 137], where active device layers are stacked vertically to achieve higher density and performance. This transition imposes unprecedented demands on the dimensional precision of materials used in chip fabrication. Organic and polymer materials, with their solution processability, chemical tunability, and potential for low-cost manufacturing, hold great promise for next-generation high-density chips. For instance, exciton diffusion length in conjugated polymer crystals is thickness-dependent: For systems with anisotropic transport, ±1 nm change in the *c*-axis dimension can shift the diffusion coefficient by up to 50%, directly impacting photovoltaic efficiency. Pioneering work by Feng and Wei has demonstrated the potential of 2D polymer semiconductors for such applications [136, 137] showing that precisely defined molecular architectures can enable high charge carrier mobility and stable device operation. However, a critical bottleneck remains: Current efforts in 2D polymer nanomaterials focus almost exclusively on in-

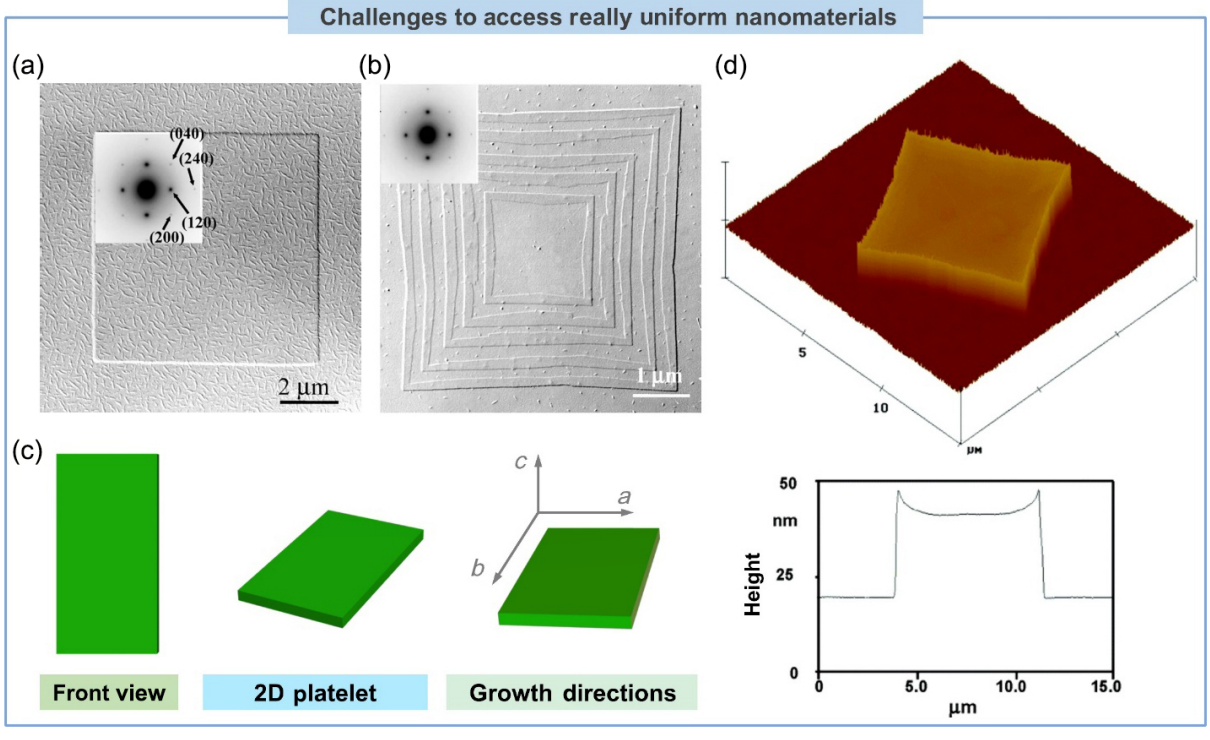

Figure 8 Challenges to access really uniform nanomaterials with low-dimensional morphologies but with 3D sizes. Single crystals formed by (a) PEO-b-PS block copolymer, and (b) alternating PEO-b-PS and homo-PEO growths. (c) Scheme to view the crystal growth directions *a*, *b* and the non-growth direction *c*. (d) The height, a typical size in non-growth direction, measured by AFM. Reproduced with permission from Ref. [134], © American Chemical Society 2004.

plane (*a*/*b*-axis) morphology control—tuning length, width, and aspect ratio. Out-of-plane (*c*-axis thickness) regulation is severely lacking. In most systems, thickness is dictated by intrinsic chain folding length at nucleation and becomes virtually immutable thereafter, as subsequent growth lacks effective sites for thickness modification [44]. This lack of thickness control translates directly into inconsistent device performance, unpredictable carrier transport pathways, and limited ability to engineer heterojunctions in vertically stacked architectures.

The fundamental origin of the difficulty lies in the intrinsic complexity of polymer crystallization. Chain folding is influenced not only by primary chain microstructure (molecular weight, dispersity, regio- and stereoregularity) but also by a host of external factors including crystallization temperature, cooling rate, solvent quality, nucleating agents, and thermal history [44–52]. Decades of polymer physics research have established that lamellar thickness is not a fixed material constant but rather a kinetically determined parameter that varies with crystallization conditions. This sensitivity, while offering some degree of tunability, also makes precise and reproducible control exceedingly challenging. Moreover, the number of nucleation events, the timing of nucleation, and the subsequent growth kinetics are often coupled, preventing independent regulation of thickness and lateral dimensions.

Thus, the field of CDSA, despite its impressive successes in controlling length, area, and even complex 3D architectures, faces a fundamental bottleneck. True three-dimensional uniformity in polymeric nanomaterials cannot be achieved without mastering the non-growth direction. Solving this problem requires a paradigm shift: from viewing chain folding as an uncontrollable kinetic outcome to treating it as a structural parameter that can be programmed by primary chain architecture. This is precisely the challenge that our work addresses in the following sections. By introducing precisely spaced folding-regulating units into polymer main chains and by designing side-chain crystallization systems where lamellar thickness is dictated by alkyl side-chain length rather than by chain folding, we demonstrate that non-growth-direction dimensions can be predicted and controlled from molecular structure upward [123, 138–140]. Achieving this capability would provide critical "materials dimension freedom" for strategic applications ranging from organic optoelectronics and semiconductor manufacturing to membrane separation and beyond.

7 Molecular design for controlling non-growth-direction dimensions

Despite the remarkable success of living CDSA in controlling the length of 1D fibers and the lateral area of 2D platelets along epitaxial growth directions, the independent regulation of *c*-axis (non-growth direction) dimensions—specifically, the diameter of 1D nanostructures and the thickness/height of 2D platelets—has remained a formidable challenge. However, recent years have witnessed emerging strategies that address this challenge through molecular design, offering new paradigms for achieving true three-dimensional control over polymeric nanomaterials. Three representative works stand out in this context, each demonstrating a distinct approach to tuning non-growth-direction dimensions.

Chen and coworkers developed a light-triggered reversible strategy to modulate the diameter of 1D wormlike nanoparticles (Fig. 9(a)) [141]. They synthesized an azobenzene-containing block copolymer, poly(methylacrylic acid)-block-poly(4-((4-butylphenyl)diazenyl) phenyl methacrylate), via PISA in ethanol. The azobenzene groups, pendant on the core-forming block, undergo reversible trans–cis isomerization upon alternative ultraviolet (UV) and visible light irradiation. In their elongated trans state, the azobenzene moieties adopt an ordered, relatively compact packing within the hydrophobic core. Upon UV irradiation, isomerization to the bent cis state disrupts this ordering, causing the core to expand and increasing the worm diameter from approximately 20 to 31 nm. Visible light irradiation reverses the process, slimming the worms back to about 23 nm. Notably, the diameter variation amplitude increases with the chain length of the core-forming block. This work demonstrates that photoresponsive molecular switches integrated into the core can dynamically and reversibly control non-growth-direction dimensions—in this case, fiber diameter—with remote, spatiotemporal precision.

Choi and colleagues tackled the thickness control of 2D nanosheets from an entirely different perspective (Fig. 9(b)) [142]. They designed a series of semiconducting polyacetylenes based on conjugated poly(1,6-heptadiyne) with bulky neohexyl-substituted fluorene side chains. Using living cyclopolymerization followed by spontaneous *in situ* nanoparticulation, these homopolymers directly formed large-area 2D nanosheets without any post-treatment. The key innovation lies in the extraordinary rigidity of the polymer backbone. Unlike flexible polymers such as polyethylene, which undergo extensive chain folding to form lamellar crystals with thickness independent of molecular weight, the rigid, extended conformation of these polyacetylenes substantially suppresses chain folding. As a result, the average height of the 2D nanosheets is directly proportional to the DP. By varying the DP from 10 to 40, the sheet height could be tuned linearly from 5 to 20 nm across three different solvents (THF, chloroform, DCM), despite the fact that the lateral shapes (leaf-like, rectangular, or raft-like) were solvent-dependent. This work provides a powerful molecular design principle: If chain folding can be suppressed through backbone rigidity, the non-growth-direction dimension becomes a predictable function of molecular weight, decoupling thickness control from external crystallization conditions.

O'Reilly, Dove, and coworkers developed an elegant post-assembly strategy to selectively modify the surface of 2D platelets in the third dimension (Fig. 9(c)) [143]. Using PCL-based block copolymers with a RAFT agent located at the corona chain end, they first constructed uniform 2D platelets via living CDSA. The key advance is the use of *in situ* light-induced polymerization—specifically photoiniferter and PET-RAFT polymerization—to grow additional polymer chains directly from the platelet surface. By controlling the concentration of DMA monomer added (from 10 to 400 mass equivalents relative to platelets), the platelet height could be precisely tuned from approximately 11 to 20 nm in a linear fashion. Importantly, because the RAFT end groups are present only on specific layers—achieved by sequential seeded growth with alternating RAFT-terminated and non-RAFT-terminated coronas—the surface modification can be spatially restricted to desired regions of a multilayered platelet. This was visualized by CLSM and STED microscopy using fluorescent monomers, revealing green ring-like patterns only on layers containing active RAFT groups. This strategy does not rely on altering polymer primary structure before assembly; rather, it exploits post-assembly

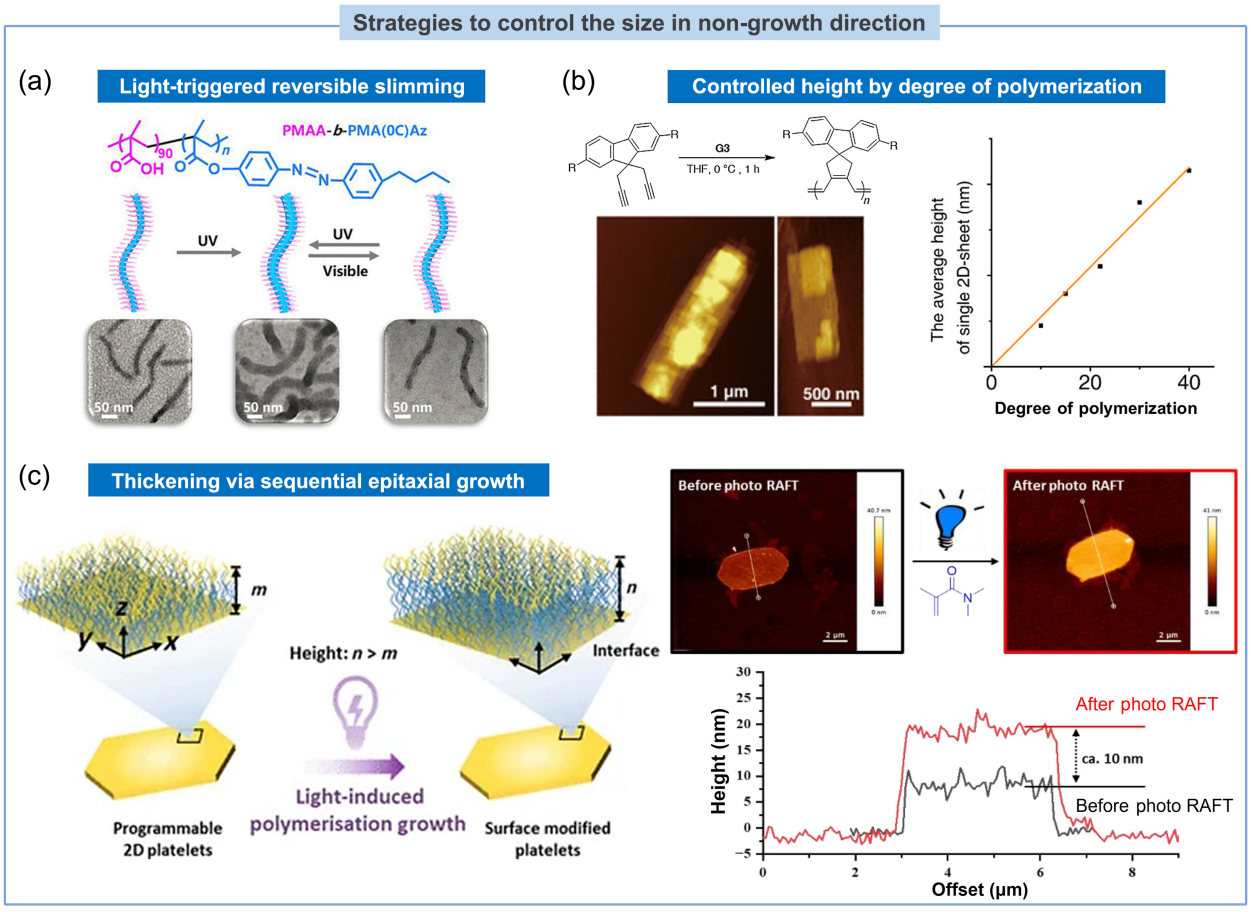

Figure 9 Current strategies to regulate the size in non-growth direction of polymeric nano-assemblies. (a) Light-triggered reversible slimming using light-responsive units-containing block copolymers. Reproduced with permission from Ref. [141], © American Chemical Society 2019. (b) Using conjugated polymers with rigid backbone leading suppressed chain-folding established relationship between the height and degree of polymerization. Reproduced with permission from Ref. [142], © American Chemical Society 2017. (c) Thickening via sequential epitaxial growth of the amorphous region through living polymerization using the RAFT agent units on the surface of nano-platelets. Reproduced with permission from Ref. [143], © Xia, T. L. et al. 2023.

polymerization from living chain ends on the platelet surface, enabling independent control over thickness and functionality while preserving the integrity of the crystalline core.

Collectively, these three representative works illuminate distinct molecular design pathways toward non-growth-direction control: photoresponsive side-group isomerization (Chen) [141], rigid backbone suppression of chain folding (Choi) [142], and post-assembly surface-initiated polymerization (O'Reilly) [143]. Each addresses the same fundamental bottleneck—the inability to regulate dimensions governed by chain folding—yet each does so through a fundamentally different mechanism. These advances have begun to shift the paradigm: from viewing non-growth-direction dimensions as uncontrollable byproducts of crystallization, to treating them as designable parameters that can be programmed through molecular architecture, backbone rigidity, or post-assembly functionalization.

Beyond these three highlighted studies, a growing body of research is exploring related strategies. For example, Schmalz and coworkers have demonstrated Janus fibers with patchy radial microphase separation using double-crystalline triblock terpolymers [144], where the radial distribution of incompatible coronas can be controlled in the non-growth direction. Zhou and colleagues systematically investigated the critical alkyl chain length for crystallization in alternating copolymers [145], revealing that chain-folding behavior emerges only when side chains exceed a certain length. Xu and co-workers demonstrated that the layer thickness of PEO single crystals along the *c*-axis can be systematically tuned by varying the molecular weight of long PEO chains [146], revealing that chain-folding behavior in the non-growth direction can be influenced by chain length under specific crystallization conditions. Tong and co-workers reported the flat-on growth of a second crystalline layer on the basal surfaces of pre-formed 2D platelets [147], achieving controlled thickening in the *c*-axis direction through secondary nucleation. This work represents an important post-assembly strategy for thickness regulation. These efforts collectively underscore that the field is moving toward a more holistic vision of polymeric nanomaterials—one where all three dimensions can be independently and predictably controlled. This emerging capability promises to unlock new applications in organic electronics, membrane separation, and nanomedicine, where thickness-dependent properties such as carrier mobility, exciton diffusion, and membrane selectivity are critically important. The convergence of molecular design, precision polymer synthesis, and advanced assembly strategies suggests that truly programmable, full-dimensional control over polymer nanomaterials may be within reach. Below we present two complementary molecular design principles that are generalizable across diverse polymer families.

8 Molecular strategies for controlling non-growth-direction dimensions via main-chain folding and side-chain crystallization

Recognizing the critical gap in controlling *c*-axis (non-growth direction) dimensions—namely, the thickness of 2D platelets and the diameter of 1D fibers—our group has developed two complementary molecular design strategies that address this challenge from fundamentally different perspectives. The first strategy focuses on controlled main-chain folding in precision polyethylene-like polymers (Fig. 10(a)) [140], where periodically spaced bulky units act as folding-regulating points to predetermine lamellar thickness. The second strategy leverages side-chain extended crystallization in polymers with long alkyl pendants, where the side-chain length serves as a direct "molecular ruler" to program crystal thickness independently of processing conditions (Fig. 10(b)) [123, 138, 139]. Together, these approaches provide a molecular-level complement to living CDSA, which excels at controlling lateral dimensions along epitaxial growth directions but cannot independently regulate thickness.

8.1 Controlled main-chain folding: Programming chain folding through precision defects

Our earlier work on precision polyethylenes established that the periodic incorporation of structural defects via acyclic diene metathesis (ADMET) polymerization profoundly influences chain packing and crystallization behavior [109–112]. Studies with arylene ether defects showed that the substitution position and size of defect units determine whether they are included in or excluded from crystalline regions, thereby affecting melting temperatures, crystallinity, and lamellar morphology. Critically, this work demonstrated that the crystallization behavior of polyethylene-like segments is not governed solely by methylene sequence length; the spatial configuration of periodic structural units along the main chain serves as an equally important variable for regulating chain folding.

Building on this mechanistic understanding, we recently introduced medium-sized cyclic and aromatic units—including cyclohexane, phenyl, and naphthalene groups—periodically into polyethylene-like main chains [110–112]. The design principle was to identify bulky groups that are large enough to be excluded from the crystalline lattice yet compact enough to mediate ordered chain folding. Among the various substitution patterns, *ortho*-disubstituted phenyl rings proved particularly effective [140]. During crystallization, these sterically hindered units are forced out of the crystalline region and act as chain-folding regulating points, guiding the intervening polyethylene segments to fold at precisely predetermined intervals.

The key finding was a strict linear relationship between lamellar thickness and the contour length of the methylene spacer between adjacent folding points. By systematically varying the spacer length from 10 to 34 methylene units (*ortho*-12C to *ortho*-34C), we obtained lamellar thicknesses ranging from approximately 1.6 to 4.5 nm, as directly measured by AFM on single crystals (Fig. 10(a)). Crucially, thickness values derived from three independent methods—AFM direct measurement, differential scanning calorimetry (DSC)-based weight-fraction calculation, and SAXS/WAXS-based volume-fraction analysis—were in excellent agreement, confirming that the crystalline core thickness is dictated by the spacer length rather than by crystallization conditions. This strategy transforms chain folding from an unpredictable kinetic outcome into a programmable structural parameter, offering a robust molecular design concept for controlling non-growth-direction dimensions in 2D polymer crystals.

8.2 Side-chain extended crystallization: The alkyl side chain as a molecular ruler

The second strategy shifts focus from main-chain folding to side-chain crystallization. Our earlier work on functionalized polyethylenes with regularly distributed ester side groups, prepared via ROMP [148, 149], revealed that side-chain crystallization can occur when the pendants are sufficiently long, and that the resulting lamellar thickness approaches the extended length of the side chain. This provided the initial rationale for using side-chain length as a tunable parameter for thickness control.

Subsequently, we developed a versatile platform based on polycyclopentene (CP) backbones bearing long, linear alkyl side chains [123, 138, 139]. This architecture offers several distinct advantages: (1) The polycyclopentene backbone is inherently depolymerizable under mild metathesis conditions, enabling closed-loop chemical recycling; (2) the low grafting density (~ 20% relative to backbone carbons) minimizes steric hindrance and facilitates ordered side-chain packing; and (3) the side chains, being polyethylene oligomers, crystallize in an extended-chain conformation without folding. By systematically varying the alkyl side-chain length from nonyl (C9) to octacosyl (C28), we achieved lamellar thicknesses in the sub-5 nm range that increase systematically with side-chain length. For CP28 (C28 side chain), AFM measurements on single crystals gave a thickness of approximately 4.75 nm, which exceeds the calculated extended chain length (~ 3.6 nm) due to the contribution of the amorphous backbone region at the crystal interfaces (Fig. 10(b)). DSC analysis using the Thomson–Gibbs equation and SAXS/WAXS volume-fraction calculations both confirmed the linear correlation between side-chain length and crystalline core thickness.

To establish a more comprehensive understanding of how backbone structure influences side-chain crystallization, we constructed a polymer library comprising six distinct backbone architectures—flexible (poly(alkyl methacrylate)s and poly(alkyl acrylate)s), rigid (polyphenylene ether derivatives), and semi-rigid (polynorbornene derivatives with single or double side chains per repeat unit, and polycyclopentene derivatives), each grafted with linear alkyl side chains ranging from decyl (C10) to triacontyl (C30) [123]. Thermal analysis revealed that for side chains shorter than C22, backbone rigidity significantly influences melting points and crystallinity. Strikingly, for side chains longer than C24, the melting points of all six polymer families converged to nearly identical values, indicating that the influence of the backbone becomes negligible when the side chains are sufficiently long. For side chains shorter than C22, the melting temperature (T_m) is influenced by the backbone rigidity because the crystallization free energy is modest and the conformational entropy penalty of the backbone contributes significantly to the overall free-energy balance. A rigid backbone imposes a higher entropic penalty during side-chain ordering, thereby lowering T_m. For side chains longer than C24, however, the side-chain crystallization enthalpy becomes sufficiently large to overwhelm the backbone conformational entropy term. As a result, the main-chain effects become negligible, and T_m is dictated almost exclusively by the side-chain length, converging to values close to those of linear polyethylene. This

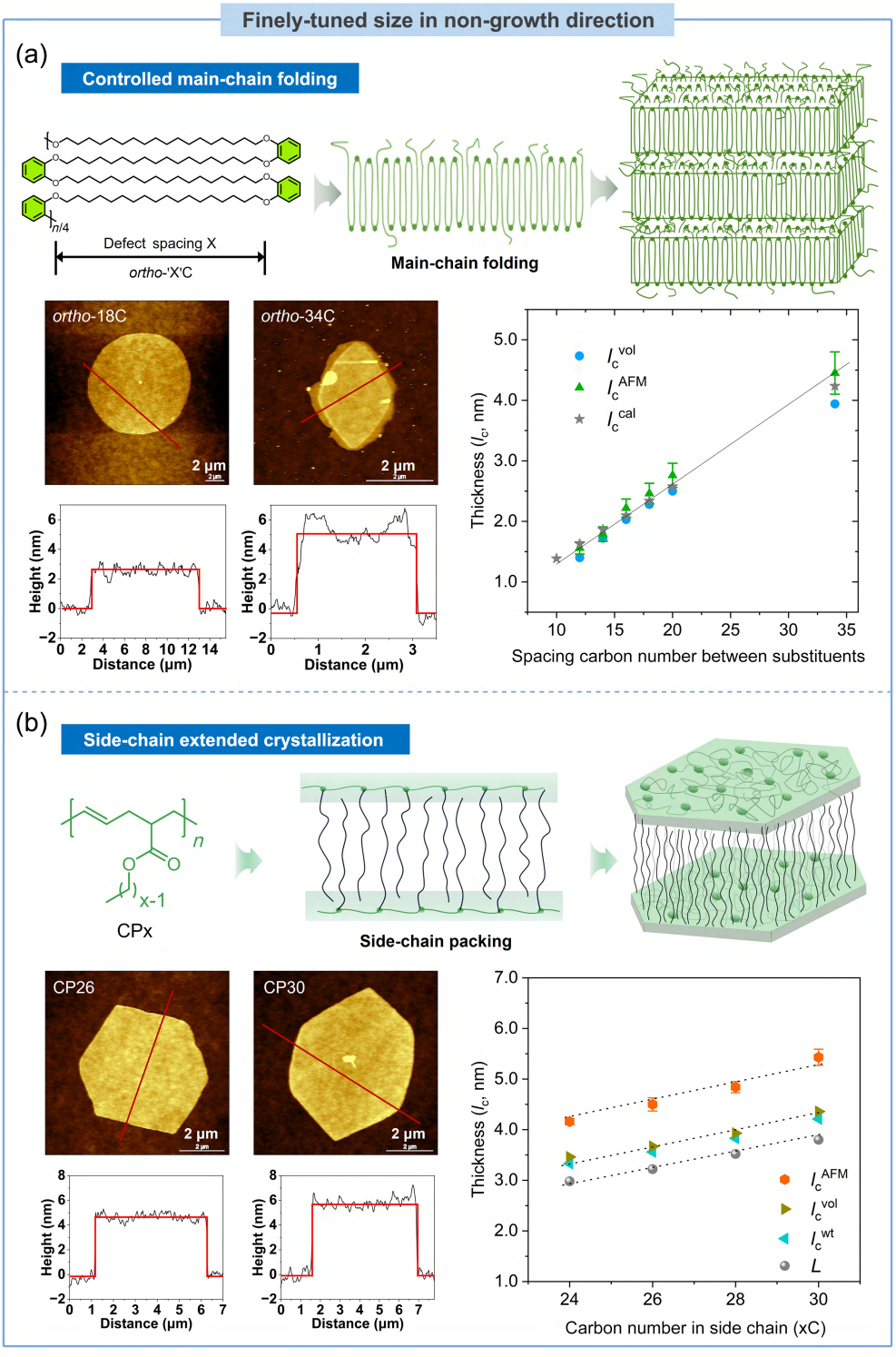

Figure 10 Molecular design for thickness control in crystalline polymeric nanomaterials. (a) Controlled main-chain folding and packing to afford controlled thickness of crystals. Reproduced with permission from Ref. [140], © American Chemical Society 2026. (b) Side-chain extended crystallization provides complementary routes to regulate non-growth-direction dimensions, especially lamellar thickness. Reproduced with permission from Ref. [123], © American Chemical Society 2026.

observation is consistent with the concept that long alkyl side chains behave as independent "polyethylene-like" nanodomains.

More importantly, the normalized lamellar thickness increased linearly with side-chain length for every polymer family, with nearly identical slopes. This universality demonstrates that extended-chain side-chain crystallization is a general phenomenon, and that side-chain length serves as a direct molecular parameter for thickness control regardless of backbone architecture. For the CP series, we further showed that crystal thickness remains invariant with changes in crystallization temperature and solution concentration, confirming that thickness is thermodynamically dictated by side-chain length rather than by kinetic processing conditions. In related

work, we extended this design concept to biomass-derived polyethylene-like plastics with recyclable backbones and long-chain crystalline side groups, demonstrating that sustainable material systems can also benefit from precise thickness control [139]. We acknowledge that the precision polymers described here are currently synthesized at gram scale. Scale-up challenges remain, but promising routes exist including continuous-flow ADMET, aqueous/emulsion ROMP, and industrial coordination catalysts offering pathways toward larger-scale production, albeit with trade-offs in sequence control.

The comparison in Table 1 reveals that both strategies achieve molecular-level thickness presetting, rendering the *c* axis dimension insensitive to crystallization conditions, a fundamental advantage over conventional CDSA. The two approaches are complementary: Main-chain folding via precision defects offers high precision in the sub 5 nm regime but requires demanding ADMET synthesis; side chain crystallization is broadly compatible with diverse backbones and more accessible polymerization methods, making it attractive for scalability. Both can be readily integrated into block copolymer designs for CDSA as discussed in the following, enabling independent control over length/width (via seeded growth) and thickness (via molecular design). Together, they constitute a versatile toolkit for achieving full-dimensional programmability.

8.3 Integration with living CDSA: Toward full three-dimensional control

Our work on controlled main-chain folding and side-chain extended crystallization can be viewed as a molecular-level complement to living CDSA. Living CDSA provides exceptional control over nanostructure length and lateral area along epitaxial growth directions, but it cannot independently regulate thickness or diameter—dimensions governed by chain folding. Our strategies address this fundamental limitation by presetting thickness at the molecular level before assembly. For main-chain folding polymers, thickness is determined by the spacing between folding-regulating units. For side-chain crystalline polymers, thickness is dictated by the extended length of alkyl pendants. In both cases, the resulting crystalline seeds have a predefined, uniform thickness that is insensitive to subsequent assembly conditions.

Looking forward, we envision that integrating these thickness-programmable polymers into block copolymer architectures will enable full three-dimensional control over nanostructure dimensions. Specifically, one can design block copolymers where the core-forming block is a thickness-programmable polymer (e.g., a CP derivative or a precision polyethylene with controlled folding), and then employ living CDSA to control lateral dimensions (length and width) via seeded growth. Alternatively, pre-formed thickness-programmable nanocrystals can serve as seeds for the epitaxial growth of compatible block copolymers. Such integration would allow independent, predictable control over length, width, and thickness—a capability that has long been sought but rarely achieved in polymeric nanomaterials. We anticipate that this combined approach will propel the field from partial size control toward truly full-dimensional programmable design of uniform polymeric nanomaterials.

The reliable assessment of *c* axis dimensions, however, requires robust characterization methods that can accurately resolve thickness at the nanometer scale. In the following section, we briefly survey the key techniques available for this purpose.

8.4 Characterization methods for *c*-axis dimensions

Accurate measurement of *c* axis dimensions—namely, the thickness of 2D platelets and the diameter of 1D fibers—is essential for validating molecular design strategies and for establishing reliable structure–property relationships. Three complementary techniques are commonly employed, each with distinct advantages and limitations.

AFM provides direct, real space measurement of individual crystal thickness (height) with sub nanometer precision. Its primary strength lies in the ability to correlate thickness with lateral morphology on a particle-by-particle basis, which is particularly valuable for assessing size distributions in a population. However, AFM is surface limited and may underreport the true crystalline core thickness due to the presence of amorphous coronas or surface contamination, and the measurement is susceptible to tip convolution artifacts.

DSC offers ensemble averaged lamellar thickness via the Thomson–Gibbs equation: $T_m = T_m^{\infty}(1 - 2\sigma_e/\Delta H_f L)$, where L is the lamellar thickness, σ_e is the surface free energy, and ΔH_f is the heat of fusion per unit volume. DSC provides statistically robust bulk information across the entire sample, but its accuracy is model dependent and requires precise knowledge of thermodynamic parameters for the specific polymer system.

Small- and wide-angle X ray scattering (SAXS/WAXS) enables determination of crystalline domain sizes via correlation function analysis (SAXS) and lattice parameters (WAXS). This approach offers statistical reliability and is nondestructive, yet it assumes a simple lamellar stack model and does not directly visualize individual objects, making it difficult to distinguish between uniform samples and mixtures of different thickness populations.

Table 1 Summary and comparison of the key features of the two molecular design strategies

Feature	Controlled main-chain folding	Side-chain extended crystallization
Mechanism	Bulky defects act as folding-regulating points	Alkyl side chains pack in extended conformation
Thickness range	~ 1.6–4.5 nm (tunable by spacer length)	~1.2–5.5 nm (tunable by alkyl chain length)
Precision	High (spacer length defines exact folding)	High (side-chain length defines exact thickness)
Compatible backbones	Polyethylene-like (ADMET)	Polycyclopentene, polynorbornene, polyacrylate, polyphenylene ether (ROMP, radical, etc.)
Advantages	Direct correlation between primary structure and lamellar thickness; highly predictable	Highly universal (applicable to diverse backbones); insensitive to crystallization conditions
Limitations	Synthetic challenge of precise defect placement; backbone-specific	Requires long side chains (≥ C12) for crystallization; lower grafting density may reduce overall crystallinity
Integration with CDSA	High potential (thickness-programmable block copolymers)	Demonstrated (CP-based block copolymers for CDSA)

In practice, we recommend that a combination of AFM (for direct visualization and distribution analysis), DSC (for thermodynamic cross validation), and SAXS/WAXS (for structural confirmation) be employed whenever possible. This multi technique approach ensures that reported *c* axis dimensions are both accurate and representative, and it is particularly important when claiming true three-dimensional uniformity in polymeric nanomaterials.

9 Conclusions and outlook

The construction of polymeric nanomaterials is undergoing a fundamental shift from empirical, trial and error preparation toward mechanism guided, rational design. For polymer soft matter systems, true "uniformity" extends far beyond simple particle size monodispersity. It must encompass three interdependent levels: uniformity in size (all three dimensions), uniformity in morphology (consistent shape across the population), and uniformity in internal structure (ordered chain packing and controlled crystalline organization). Achieving this holistic uniformity is essential for establishing reliable structure–property relationships and for translating laboratory discoveries into practical applications.

Conventional top-down strategies, despite their scalability, remain inherently limited in their ability to produce nano objects with intact internal order, narrow size distributions, and predictable architectures. By contrast, bottom-up strategies offer mechanism level control over nucleation, phase separation, spatial confinement, self-assembly, and crystal growth. Among bottom-up methods, polymerization-based formation routes (e.g., PISA, bottlebrush synthesis) couple chain growth with nanostructure formation. While efficient for spheres, worms, and vesicles, they struggle to achieve predictable, independent control over dimensions of low curvature anisotropic structures. Preformed polymer assembly routes, particularly solvent mediated particle formation, are versatile for spherical carriers but lack the ability to generate highly ordered, size-predictable anisotropic nanomaterials. Among molecular self-organization routes, CDSA stands out as the most powerful platform for achieving morphological diversification, high internal order, and predictable size regulation. The development of living CDSA—through seeded growth and self-seeding—has successfully decoupled nucleation from growth, enabling unprecedented control over nanostructure length, lateral area, and spatial composition along epitaxial growth directions.

To contextualize the evolution of this field and to highlight the progressive refinement of dimensional control, we present a schematic timeline of key milestones in CDSA and its associated molecular design strategies in Fig. 11. The journey began in the 1950s–1960s with the establishment of the chain folding concept in polymer single crystals (Keller; Fischer) [150–152], which laid the molecular foundation for understanding lamellar thickness. The first block copolymer CDSA was reported in 1998 by Manners and Winnik [9], followed by the breakthrough of living seeded growth (2007) and self seeding (2011) [12, 13], which enabled predictable control over length and lateral area along epitaxial growth directions. The subsequent decade witnessed the emergence of 2D platelets (2016–2017) and complex 3D architectures such as spherulitic micelles (2021) [67, 114–116, 120] demonstrating the expanding morphological toolbox of CDSA. Most recently, the period of 2025–2026 has seen the rise of molecular design strategies including controlled main chain folding, side chain extended crystallization, and complementary approaches by Chen, Choi, and O'Reilly that target the long overlooked *c* axis (non growth direction) [141–143]. This timeline visually anchors the narrative and underscores that the field is now poised at a critical juncture: moving from empirical size control toward truly programmable, full dimensional precision.

However, despite these impressive advances, a critical bottleneck remains: the inability to independently control dimensions in the non growth direction (*c* axis)—namely, the diameter of 1D fibers and the thickness/height of 2D platelets. While living CDSA provides exceptional predictability along *a*/*b* axes, the *c* axis dimension is governed by polymer chain folding, a process historically viewed as an unpredictable kinetic outcome of crystallization conditions. This gap has been largely overlooked in the CDSA literature, where "uniformity" is often claimed based solely on length or area distributions, while thickness or diameter distributions remain unaddressed or uncharacterized.

What distinguishes our review from existing comprehensive surveys is our focused and critical examination of this overlooked third dimension. Recent reviews such as Müllner et al. (Chem. Soc. Rev. 2024) on discs, toroids, and platelets [153], O'Reilly et al. (Chem. Rev. 2025) on CDSA evolution and characterization [33], and Stenzel et al. (Prog. Polym. Sci. 2020) on living CDSA concepts [19] have provided excellent overviews of morphology control, assembly mechanisms, and applications. However, none of these reviews have placed the challenge of non growth direction control as a central, unifying theme. This review work uniquely:

(1) Identifies the non-growth direction as the critical frontier in CDSA and polymer nanomaterial design, systematically explaining why *c*-axis control is fundamentally harder than a/b-axis control.

(2) Surveys emerging strategies (Chen, Choi, O'Reilly) [141–143] and presents our own molecular design approaches, controlled main-chain folding via precision defects and side-chain extended crystallization, that enable programmable thickness control.

(3) Demonstrates that non-growth-direction dimensions can be programmed at the molecular level, transforming thickness from a processing-sensitive parameter into a predictable structural feature determined by primary chain architecture.

Our work shows that two complementary molecular strategies enable predictable *c* axis control. First, by periodically incorporating

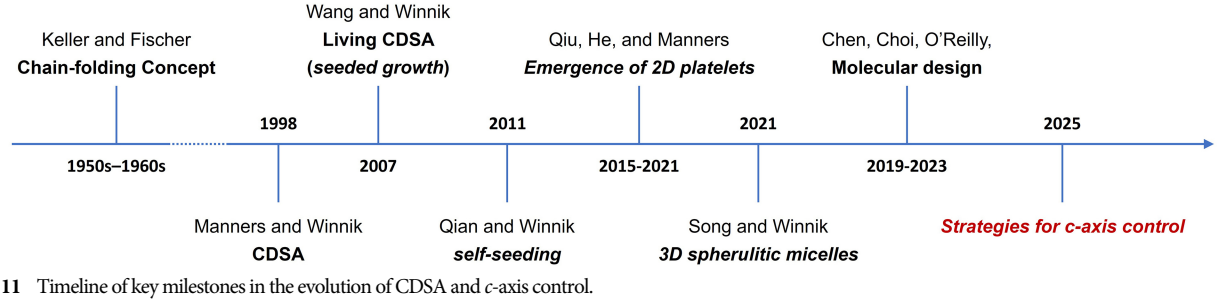

Figure 11 Timeline of key milestones in the evolution of CDSA and *c*-axis control.

ortho-disubstituted cyclic or aromatic units into a polyethylene like main chain, these bulky groups are excluded from the crystalline lattice and act as chain folding regulating points. Lamellar thickness then scales linearly with the spacing between adjacent defects, a direct manifestation of "chain folding by design." Second, in side-chain crystalline polymers based on a recyclable polycyclopentene backbone, long alkyl side chains pack in an extended chain conformation without folding. Lamellar thickness is determined solely by side chain length, is tunable from 1.2 to 5.5 nm, and is remarkably insensitive to crystallization temperature and solution concentration, a true "molecular ruler" for thickness.

Looking forward, we envision that the integration of living CDSA (for *a*/*b* axis control) with these molecular design strategies (for *c* axis control) will enable true three-dimensional programmability of polymeric nanomaterials. Future research should focus on (Fig. 12): (1) extending these molecular design principles to other semicrystalline polymer systems (e.g., polyesters, polycarbonates) to expand the toolbox of thickness programmable cores; (2) incorporating thickness programmable homopolymers or block copolymers into living CDSA seeded growth protocols, thereby combining independent control over length, width, and thickness; (3) developing scalable, robust, and reproducible preparation methods that move beyond dilute-solution constraints, a major current bottleneck, as conventional CDSA relies on low polymer concentrations (typically < 0.1 wt.%) and sonication-based seed preparation, which are difficult to scale, potentially through continuous-flow CDSA or polymerization-induced CDSA with pre-designed thickness control; and (4) establishing comprehensive characterization standards that report all three dimensions (length × width × height or diameter × thickness) with quantitative distributions, moving beyond the current practice of emphasizing only lateral dimensions. For instance, for 1D fibers: report length and diameter distributions, both with number-averaged values (L_n, d_n) and dispersity indices ($Đ_L$, $Đ_d$), obtained from TEM and AFM, respectively. For 2D platelets: report length, width, and height/thickness distributions (L_n, W_n, H_n) with corresponding dispersity indices ($Đ_L$, $Đ_W$, $Đ_H$), obtained from TEM (length and width) and AFM (height), with at least 100 objects counted per sample. For all cases: specify the number of objects counted, the imaging conditions, and the statistical methods used.

Ultimately, the value of uniform polymeric nanomaterials lies not only in their structural perfection but in their functional integration (Fig. 12). By combining full dimensional structural control with stimuli responsiveness, biological function, interfacial recognition, and multicomponent integration, polymer nanomaterials can evolve from "structurally controlled nano objects" into truly programmable soft matter nanosystems with predictable behavior and broad application potential in biomedicine, optoelectronics, catalysis, and sustainable materials [2, 154–157]. Our review provides a roadmap for achieving this vision—by placing the long overlooked third dimension at the center of the design paradigm.

Data availability

This study did not generate new data and code.

Acknowledgements

Financial support from the National Natural Science Foundation of China (No. 52473011), the Fundamental Research Funds for the Central Universities (Nos. 226-2025-00130 and 226-2025-00031), State Key Laboratory (SKL) of Biobased Transportation Fuel Technology, and International Scientific Research Cooperation Seed Fund of International Campus (Zhejiang University) is gratefully acknowledged.

Declaration of competing interest

The authors declare no competing financial interest.

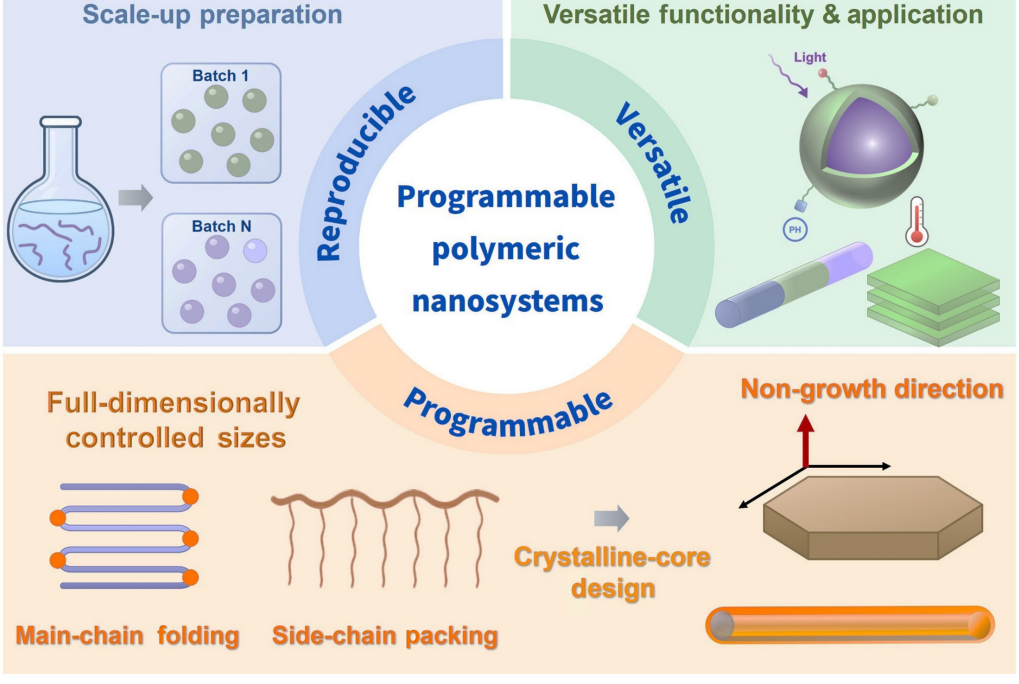

Figure 12 Perspectives on uniform polymeric nanomaterials. Future development may focus on full-dimensional structural control, robust and reproducible preparation, and versatile functional integration/applications.

Author contribution statement

E. F.: Conceptualization, data curation, formal analysis, investigation, writing – original draft, writing – review & editing. L. Y. C., Z. J. H., W. M. W., and J. T. X.: Formal analysis, investigation, writing – original draft. S. F. S.: Conceptualization, funding acquisition, supervision, writing – review & editing.

Use of AI statement

None.

References

[1] Elsabahy, M.; Wooley, K. L. Design of polymeric nanoparticles for biomedical delivery applications. *Chem. Soc. Rev.* **2012**, *41*, 2545–2561.

[2] MacFarlane, L.; Zhao, C. Q.; Cai, J. D.; Qiu, H. B.; Manners, I. Emerging applications for living crystallization-driven self-assembly. *Chem. Sci.* **2021**, *12*, 4661–4682.

[3] Mitchell, M. J.; Billingsley, M. M.; Haley, R. M.; Wechsler, M. E.; Peppas, N. A.; Langer, R. Engineering precision nanoparticles for drug delivery. *Nat. Rev. Drug Discov.* **2021**, *20*, 101–124.

[4] Beach, M. A.; Nayanathara, U.; Gao, Y. T.; Zhang, C. H.; Xiong, Y. J.; Wang, Y. F.; Such, G. K. Polymeric nanoparticles for drug delivery. *Chem. Rev.* **2024**, *124*, 5505–5616.

[5] Gast, A. P.; Vinson, P. K.; Cogan-Farinas, K. A. An intriguing morphology in crystallizable block copolymers. *Macromolecules* **1993**, *26*, 1774–1776.

[6] Lin, E. K.; Gast, A. P. Semicrystalline diblock copolymer platelets in dilute solution. *Macromolecules* **1996**, *29*, 4432–4441.

[7] Mai, Y.; Eisenberg, A. Self-assembly of block copolymers. *Chem. Soc. Rev.* **2012**, *41*, 5969–5985.

[8] Gröschel, A. H.; Müller, A. H. E. Self-assembly concepts for multicompartment nanostructures. *Nanoscale* **2015**, *7*, 11841–11876.

[9] Massey, J.; Power, K. N.; Manners, I.; Winnik, M. A. Self-assembly of a novel organometallic-inorganic block copolymer in solution and the solid state: Nonintrusive observation of novel wormlike poly(ferrocenyldimethylsilane)-*b*-poly(dimethylsiloxane) micelles. *J. Am. Chem. Soc.* **1998**, *120*, 9533–9540.

[10] Raez, J.; Barjovanu, R.; Massey, J. A.; Winnik, M. A.; Manner, I. Self-assembled organometallic block copolymer nanotubes. *Angew. Chem., Int. Ed.* **2000**, *39*, 3862–3865.

[11] Cao, L.; Manners, I.; Winnik, M. A. Influence of the interplay of crystallization and chain stretching on micellar morphologies: Solution self-assembly of coil-crystalline poly(isoprene-*block*-ferrocenylsilane). *Macromolecules* **2002**, *35*, 8258–8260.

[12] Wang, X. S.; Guerin, G.; Wang, H.; Wang, Y. S.; Manners, I.; Winnik, M. A. Cylindrical block copolymer micelles and co-micelles of controlled length and architecture. *Science* **2007**, *317*, 644–647.

[13] Qian, J. S.; Guerin, G.; Lu, Y. J.; Cambridge, G.; Manners, I.; Winnik, M. A. Self-seeding in one dimension: An approach to control the length of fiberlike polyisoprene-polyferrocenylsilane block copolymer micelles. *Angew. Chem., Int. Ed.* **2011**, *50*, 1622–1625.

[14] He, W. N.; Xu, J. T. Crystallization assisted self-assembly of semicrystalline block copolymers. *Prog. Polym. Sci.* **2012**, *37*, 1350–1400.

[15] Inam, M.; Cambridge, G.; Pitto-Barry, A.; Laker, Z. P. L.; Wilson, N. R.; Mathers, R. T.; Dove, A. P.; O'Reilly, R. K. 1D vs. 2D shape selectivity in the crystallization-driven self-assembly of polylactide block copolymers. *Chem. Sci.* **2017**, *8*, 4223–4230.

[16] Cai, J. D.; Li, C.; Kong, N.; Lu, Y.; Lin, G. Y.; Wang, X. Y.; Yao, Y.; Manners, I.; Qiu, H. B. Tailored multifunctional micellar brushes via crystallization-driven growth from a surface. *Science* **2019**, *366*, 1095–1098.

[17] Wang, Z. H.; Fang, E.; He, Z. J.; Fan, Z. Q.; Song, S. F. Controlling polymer crystallization with bulky chiral substituents: Steric effects, chirality transfer, and three-dimensional size control. *Macromolecules* **2026**, *59*, 7057–7067.

[18] Yang, S.; Choi, T. L. Rapid formation and real-time observation of micron-sized conjugated nanofibers with tunable lengths and widths in 20 minutes by living crystallization-driven self-assembly. *Chem. Sci.* **2020**, *11*, 8416–8424.

[19] Ganda, S.; Stenzel, M. H. Concepts, fabrication methods and applications of living crystallization-driven self-assembly of block copolymers. *Prog. Polym. Sci.* **2020**, *101*, 101195.

[20] Song, S. F.; Liu, X. M.; Nikbin, E.; Howe, J. Y.; Yu, Q.; Manners, I.; Winnik, M. A. Uniform 1D micelles and patchy & block comicelles via scalable, one-step crystallization-driven block copolymer self-assembly. *J. Am. Chem. Soc.* **2021**, *143*, 6266–6280.

[21] Song, S. F.; Zhou, H.; Manners, I.; Winnik, M. A. Block copolymer self-assembly: Polydisperse corona-forming blocks leading to uniform morphologies. *Chem* **2021**, *7*, 2800–2821.

[22] Lin, G. Y.; Cai, J. D.; Sun, Y.; Cui, Y.; Liu, Q. W.; Manners, I.; Qiu, H. B. Capillary-bound dense micelle brush supports for continuous flow catalysis. *Angew. Chem., Int. Ed.* **2021**, *60*, 24637–24643.

[23] Hils, C.; Manners, I.; Schöbel, J.; Schmalz, H. Patchy micelles with a crystalline core: Self-assembly concepts, properties, and applications. *Polymers* **2021**, *13*, 1481.

[24] Tang, Z. M.; Gao, L.; Lin, J. P.; Cai, C. H.; Yao, Y.; Guerin, G.; Tian, X. H.; Lin, S. L. Anchorage-dependent living supramolecular self-assembly of polymeric micelles. *J. Am. Chem. Soc.* **2021**, *143*, 14684–14693.

[25] Jin, X.; Zhang, C. Y.; Lin, J. P.; Cai, C. H.; Chen, J. D.; Gao, L. Fusion growth of two-dimensional disklike micelles via liquid-crystallization-driven self-assembly. *Macromolecules* **2022**, *55*, 3831–3839.

[26] Hu, L. J.; Li, Q.; Luo, Y. J.; Jin, B. X.; Chi, S. M.; Li, X. Y. Controllable one-step assembly of uniform liquid crystalline block copolymer cylindrical micelles by a tailored nucleation-growth process and their application as toughening. *Angew. Chem., Int. Ed.* **2023**, *62*, e202310022.

[27] Tong, Z. Z.; Xie, Y. J.; Arno, M. C.; Zhang, Y. F.; Manners, I.; O'Reilly, R. K.; Dove, A. P. Uniform segmented platelet micelles with compositionally distinct and selectively degradable cores. *Nat. Chem.* **2023**, *15*, 824–831.

[28] Teng, F. Y.; Xiang, B. B.; Liu, L. P.; Varlas, S.; Tong, Z. Z. Precise control of two-dimensional hexagonal platelets via scalable, one-pot assembly pathways using block copolymers with crystalline side chains. *J. Am. Chem. Soc.* **2023**, *145*, 28049–28060.

[29] Lin, G. Y.; Tao, J. W.; Sun, Y.; Cui, Y.; Manners, I.; Qiu, H. B. Breaking of lateral symmetry in two-dimensional crystallization-driven self-assembly on a surface. *J. Am. Chem. Soc.* **2024**, *146*, 14734–14744.

[30] Zhang, J. C.; Xiao, T. Y.; Liu, Z. L.; Yin, Y. C.; Li, C.; Xu, F. G.; Mai, Y. Area-controllable nanoplatelets from rapid photocontrolled living crystallization-driven self-assembly of an alternating copolymer. *J. Am. Chem. Soc.* **2025**, *147*, 19148–19156.

[31] Xiao, L. H.; Xia, T. L.; Zhang, J.; Parkinson, S. J.; Rho, J. Y.; Dove, A. P.; O'Reilly, R. K. Direct preparation of two-dimensional platelets from polymers enabled by accelerated seed formation. *Nat. Synth.* **2025**, *4*, 808–815.

[32] Yu, X. L.; Fang, Y. J.; Luo, Z. R.; Guo, X. J.; Fu, L. L.; Fan, Z.; Zhao, J.; Xie, H. X.; Guo, M. J.; Cheng, B. W. Precise preparation of size-uniform two-dimensional platelet micelles through crystallization-assisted rapid microphase separation using all-bottlebrush-type block copolymers with crystalline side chains. *J. Am. Chem. Soc.* **2025**, *147*, 2193–2205.

[33] Xia, T. L.; Xiao, L. H.; Xie, Y. J.; Dove, A. P.; O'Reilly, R. K. Deciphering evolution, function, and observation of crystallization-driven self-assembly. *Chem. Rev.* **2025**, *125*, 10105–10178.

[34] Li, M. C.; Ma, Y. X.; Li, J.; Zhang, X. L.; Xu, Z. H.; Shi, A. C.; Liu,

B. Uniform single-domain liquid crystalline hexagonal rods by synchronized polymerization and self-assembly using disc-shaped monomers. *J. Am. Chem. Soc.* **2025**, *147*, 10401–10412.

[35] Cai, J. D.; Chua, X. W.; Li, C.; Grüne, J.; Ghosh, P.; Ding, Y. F.; MacKenzie, H. K.; Qiu, H. B.; Greenham, N. C.; Rao, A. et al. Uniform conjugated polymer rectangular platelets exhibiting long-range exciton diffusion. *Nat. Mater.* **2025**, *24*, 1985–1992.

[36] Chen, R.; Zhang, S.; Huang, X. Y.; Lu, G. L.; Winnik, M. A.; Feng, C. Near infrared light regulated crystallization-driven self-assembly: A versatile platform for controlled preparation of uniform π-conjugated functional nanostructures. *Chem. Sci.* **2026**, *17*, 9454–9467.

[37] Rao, J. P.; Geckeler, K. E. Polymer nanoparticles: Preparation techniques and size-control parameters. *Prog. Polym. Sci.* **2011**, *36*, 887–913.

[38] Deng, R. H.; Mao, X.; Pearce, S.; Tian, J.; Zhang, Y. F.; Manners, I. Role of competitive crystallization kinetics in the formation of 2D platelets with distinct coronal surface patterns via seeded growth. *J. Am. Chem. Soc.* **2022**, *144*, 19051–19059.

[39] Fan, B.; Wang, R. Y.; Wang, X. Y.; Xu, J. T.; Du, B. Y.; Fan, Z. Q. Crystallization-driven co-assembly of micrometric polymer hybrid single crystals and nanometric crystalline micelles. *Macromolecules* **2017**, *50*, 2006–2015.

[40] Guo, X. S.; Zhang, Z. K.; Zhang, T. Y.; Tong, Z. Z.; Xu, J. T.; Fan, Z. Q. Interfacial self-assembly of amphiphilic conjugated block copolymer into 2D nanotapes. *Soft Matter* **2019**, *15*, 8790–8799.

[41] Song, S. F.; Yu, Q.; Zhou, H.; Hicks, G.; Zhu, H.; Rastogi, C. K.; Manners, I.; Winnik, M. A. Solvent effects leading to a variety of different 2D structures in the self-assembly of a crystalline-coil block copolymer with an amphiphilic corona-forming block. *Chem. Sci.* **2020**, *11*, 4631–4643.

[42] Song, S. F.; Zhou, H.; Hicks, G.; Jiang, J. J.; Zhang, Y. F.; Manners, I.; Winnik, M. A. An amphiphilic corona-forming block promotes formation of a variety of 2D platelets via crystallization-driven block copolymer self-assembly. *Macromolecules* **2021**, *54*, 9761–9772.

[43] Reiter, G. Some unique features of polymer crystallisation. *Chem. Soc. Rev.* **2014**, *43*, 2055–2065.

[44] Hu, W. B. The physics of polymer chain-folding. *Phys. Rep.* **2018**, *747*, 1–50.

[45] Zhang, J.; Hu, W. B. Double-lamella phenomenon of once-folding polymer crystallization raised by chain-end hydrogen-bonding interactions. *Polymer* **2023**, *281*, 126089.

[46] Tang, X. L.; Chen, W.; Li, L. B. The tough journey of polymer crystallization: Battling with chain flexibility and connectivity. *Macromolecules* **2019**, *52*, 3575–3591.

[47] Marxsen, S. F.; Häußler, M.; Mecking, S.; Alamo, R. G. Isothermal step thickening in a long-spaced aliphatic polyester. *Polymer* **2020**, *191*, 122282.

[48] Haider, T.; Suraeva, O.; O'Duill, M. L.; Mars, J.; Mezger, M.; Lieberwirth, I.; Wurm, F. R. Controlling the crystal structure of precisely spaced polyethylene-like polyphosphoesters. *Polym. Chem.* **2020**, *11*, 3404–3415.

[49] Li, L.; Hu, J.; Li, Y. P.; Huang, Q. G.; Sun, X. L.; Yan, S. K. Evidence for the soft and hard epitaxies of poly(L-lactic acid) on an oriented polyethylene substrate and their dependence on the crystallization temperature. *Macromolecules* **2020**, *53*, 1745–1751.

[50] Wang, Z. F.; Dong, X.; Cavallo, D.; Wang, D. J.; Müller, A. J. Peculiar self-nucleation behavior of a polybutene-1/ethylene random copolymer. *Polym. Cryst.* **2021**, *4*, e10201.

[51] Shi, H. F.; Zhao, Y.; Dong, X.; Zhou, Y.; Wang, D. J. Frustrated crystallisation and hierarchical self-assembly behaviour of comb-like polymers. *Chem. Soc. Rev.* **2013**, *42*, 2075–2099.

[52] Shi, H. F.; Wang, H. X.; Xin, J. H.; Zhang, X. X.; Wang, D. J. Nanoconfinement crystallization of frustrated alkyl groups: Crossover of mesophase to crystalline structure. *Chem. Commun.* **2011**, *47*, 3825–3827.

[53] Xu, W. Q.; Zheng, Y.; Pan, P. J. Crystallization-driven self-assembly of semicrystalline block copolymers and end-functionalized polymers: A minireview. *J. Polym. Sci.* **2022**, *60*, 2136–2152.

[54] Yang, C.; Li, Z. X.; Xu, J. T. Single crystals and two-dimensional crystalline assemblies of block copolymers. *J. Polym. Sci.* **2022**, *60*, 2153–2174.

[55] Tao, J. W.; Lu, Y.; Gao, C. C.; Wang, P. W.; Ji, Z. Y.; Lv, S.; Cai, X. M.; Zhang, J. W.; Qiu, H. B. Surface-initiated living crystallization-driven self-assembly: From precision nanofabrication to functional interfaces. *Chem. Soc. Rev.* **2026**, *55*, 4031–4053.

[56] Rolland, J. P.; Maynor, B. W.; Euliss, L. E.; Exner, A. E.; Denison, G. M.; DeSimone, J. M. Direct fabrication and harvesting of monodisperse, shape-specific nanobiomaterials. *J. Am. Chem. Soc.* **2005**, *127*, 10096–10100.

[57] Li, Z. L.; Lin, Z. Q. Two-dimensional polymers: Synthesis and applications. *ACS Appl. Mater. Interfaces* **2021**, *13*, 45130–45138.

[58] Perry, J. L.; Herlihy, K. P.; Napier, M. E.; DeSimone, J. M. PRINT: A novel platform toward shape and size specific nanoparticle theranostics. *Acc. Chem. Res.* **2011**, *44*, 990–998.

[59] Xu, J.; Wong, D. H. C.; Byrne, J. D.; Chen, K.; Bowerman, C.; DeSimone, J. M. Future of the particle replication in nonwetting templates (PRINT) technology. *Angew. Chem., Int. Ed.* **2013**, *52*, 6580–6589.

[60] Tripathy, S.; Rodrigues, J.; Shimpi, N. G. Top-down and bottom-up approaches for synthesis of nanoparticles. *Mater. Res. Proc.* **2023**, *145*, 92–130.

[61] Luo, C.; Wang, Q.; Zhang, L. K.; Xia, J.; Liang, H. L.; Chu, J. H. *In situ* structural engineering of two-dimensional nanomaterials at atomic scale. *Mater. Sci. Eng.: B* **2026**, *323*, 118717.

[62] Jung, Y.; Kline, R. J.; Fischer, D. A.; Lin, E. K.; Heeney, M.; McCulloch, I.; Delongchamp, D. M. The effect of interfacial roughness on the thin film morphology and charge transport of high-performance polythiophenes. *Adv. Funct. Mater.* **2008**, *18*, 742–750.

[63] Korevaar, P. A.; George, S. J.; Markvoort, A. J.; Smulders, M. M. J.; Hilbers, P. A. J.; Schenning, A. P. H. J.; De Greef, T. F. A.; Meijer, E. W. Pathway complexity in supramolecular polymerization. *Nature* **2012**, *481*, 492–496.

[64] Cote, A. P.; Benin, A. I.; Ockwig, N. W.; O'Keeffe, M.; Matzger, A. J.; Yaghi, O. M. Porous, crystalline, covalent organic frameworks. *Science* **2005**, *310*, 1166–1170.

[65] Lyle, S. J.; Waller, P. J.; Yaghi, O. M. Covalent organic frameworks: Organic chemistry extended into two and three dimensions. *Trends Chem.* **2019**, *1*, 172–184.

[66] Xu, X. Y.; Huang, N. Multicomponent covalent organic frameworks: Design strategies and synergistic functions. *Chem. Sci.* **2025**, *16*, 17034–17057.

[67] Han, L.; Wang, M. J.; Jia, X. M.; Chen, W.; Qian, H. J.; He, F. Uniform two-dimensional square assemblies from conjugated block copolymers driven by π–π interactions with controllable sizes. *Nat. Commun.* **2018**, *9*, 865.

[68] Song, S. F.; Xu, J. T.; Zhou, H.; Manners, I.; Winnik, M. A. Focal point association of core-crystalline micelles with an amphiphilic corona block. *J. Am. Chem. Soc.* **2025**, *147*, 9919–9930.

[69] Schaller, R.; Foith, M.; Günther, L. M.; Hund, M.; Busse, K.; Karg, M.; Schmalz, H. From Janus spheres to twisted patchy platelets and their 3D assemblies by Co-crystallization-driven self-assembly. *Macromolecules* **2026**, *59*, 3092–3103.

[70] Canning, S. L.; Smith, G. N.; Armes, S. P. A critical appraisal of RAFT-mediated polymerization-induced self-assembly. *Macromolecules* **2016**, *49*, 1985–2001.

[71] Derry, M. J.; Fielding, L. A.; Armes, S. P. Polymerization-induced self-assembly of block copolymer nanoparticles via RAFT non-aqueous dispersion polymerization. *Prog. Polym. Sci.* **2016**, *52*, 1–18.

[72] Pesek, S. L.; Li, X. Y.; Hammouda, B.; Hong, K. L.; Verduzco, R.

Small-angle neutron scattering analysis of bottlebrush polymers prepared via grafting-through polymerization. *Macromolecules* **2013**, *46*, 6998–7005.

[73] Penfold, N. J. W.; Yeow, J.; Boyer, C.; Armes, S. P. Emerging trends in polymerization-induced self-assembly. *ACS Macro Lett.* **2019**, *8*, 1029–1054.

[74] Wang, X.; An, Z. S. New insights into RAFT dispersion polymerization-induced self-assembly: From monomer library, morphological control, and stability to driving forces. *Macromol. Rapid Commun.* **2019**, *40*, 1800325.

[75] Mitchell, D. E.; Lovett, J. R.; Armes, S. P.; Gibson, M. I. Combining biomimetic block copolymer worms with an ice-inhibiting polymer for the solvent-free cryopreservation of red blood cells. *Angew. Chem., Int. Ed.* **2016**, *55*, 2801–2804.

[76] Dai, X. C.; Yu, L. L.; Zhang, Y. X.; Zhang, L.; Tan, J. B. Polymerization-induced self-assembly via RAFT-mediated emulsion polymerization of methacrylic monomers. *Macromolecules* **2019**, *52*, 7468–7476.

[77] Liu, D. D.; Cai, W. B.; Zhang, L.; Boyer, C.; Tan, J. B. Efficient photoinitiated polymerization-induced self-assembly with oxygen tolerance through dual-wavelength type I photoinitiation and photoinduced deoxygenation. *Macromolecules* **2020**, *53*, 1212–1223.

[78] Lin, D. N.; Li, Y. L.; Zhang, L.; Chen, Y.; Tan, J. B. Scalable preparation of cylindrical block copolymer micelles with a liquid-crystalline perfluorinated core by photoinitiated reversible addition-fragmentation chain transfer dispersion polymerization. *Macromolecules* **2023**, *56*, 440–447.

[79] Wang, C.; Zhao, H. Y. Polymer brushes and surface nanostructures: Molecular design, precise synthesis, and self-assembly. *Langmuir* **2024**, *40*, 2439–2464.

[80] Du, R. L.; Fielding, L. A. pH-responsive nanogels generated by polymerization-induced self-assembly of a succinate-functional monomer. *Macromolecules* **2024**, *57*, 3496–3501.

[81] Sugihara, S.; Tsutsui, Y.; Uematsu, H.; Matsumoto, A.; Maeda, Y. Synthesis of flower-like micelles that recognize thermal history via RAFT aqueous dispersion polymerization. *Macromolecules* **2024**, *57*, 4524–4535.

[82] Zhou, P.; Shi, B. Y.; Zhang, J. W.; Shen, D.; Li, D.; Liang, X. Y.; Wang, G. W. Phenolic formaldehyde resin-based nano-objects via a modification-induced cooperative assembly process using poly(4-hydroxystyrene) as the core-forming block. *Macromolecules* **2025**, *58*, 11123–11136.

[83] Xia, T. C.; Zhang, T. H.; Huo, M. Sulfone-modulated aqueous polymerization-induced self-assembly: Tailoring adaptive nanostructures via competing supramolecular interactions. *Langmuir* **2025**, *41*, 10011–10019.

[84] Wang, C.; Liu, Q. Y.; Ye, C. C.; Du, X. H.; Xu, L. Enhanced accessibility and stability of worm-like micelles via ring-opening metathesis polymerization-induced self-assembly. *Macromolecules* **2026**, *59*, 5924–5932.

[85] Fang, R.; Chen, Z. Y.; Liu, B. R.; Zhang, G. J.; Li, D. Z.; Wang, H. L.; Sun, J.; Chen, X. S. Polymerization-induced chiral supramolecular polypeptide hydrogels for enhanced mechanical property and selective bioactivity. *Macromolecules* **2026**, *59*, 3003–3013.

[86] Xia, Y.; Olsen, B. D.; Kornfield, J. A.; Grubbs, R. H. Efficient synthesis of narrowly dispersed brush copolymers and study of their assemblies: The importance of side chain arrangement. *J. Am. Chem. Soc.* **2009**, *131*, 18525–18532.

[87] Sun, G. R.; Cho, S.; Clark, C.; Verkhoturov, S. V.; Eller, M. J.; Li, A.; Pavía-Jiménez, A.; Schweikert, E. A.; Thackeray, J. W.; Trefonas, P. et al. Nanoscopic cylindrical dual concentric and lengthwise block brush terpolymers as covalent preassembled high-resolution and high-sensitivity negative-tone photoresist materials. *J. Am. Chem. Soc.* **2013**, *135*, 4203–4206.

[88] Cai, L. H.; Kodger, T. E.; Guerra, R. E.; Pegoraro, A. F.; Rubinstein, M.; Weitz, D. A. Soft poly(dimethylsiloxane) elastomers from architecture-driven entanglement free design. *Adv. Mater.* **2015**, *27*, 5132–5140.

[89] Daniel, W. F. M.; Burdyńska, J.; Vatankhah-Varnoosfaderani, M.; Matyjaszewski, K.; Paturej, J.; Rubinstein, M.; Dobrynin, A. V.; Sheiko, S. S. Solvent-free, supersoft and superelastic bottlebrush melts and networks. *Nat. Mater.* **2016**, *15*, 183–189.

[90] Foster, J. C.; Varlas, S.; Couturaud, B.; Coe, Z.; O'Reilly, R. K. Getting into shape: Reflections on a new generation of cylindrical nanostructures' self-assembly using polymer building blocks. *J. Am. Chem. Soc.* **2019**, *141*, 2742–2753.

[91] Varlas, S.; Keogh, R.; Xie, Y. J.; Horswell, S. L.; Foster, J. C.; O'Reilly, R. K. Polymerization-induced polymersome fusion. *J. Am. Chem. Soc.* **2019**, *141*, 20234–20248.

[92] Li, Z. L.; Tang, M.; Liang, S.; Zhang, M. Y.; Biesold, G. M.; He, Y. J.; Hao, S. M.; Choi, W.; Liu, Y. J.; Peng, J. et al. Bottlebrush polymers: From controlled synthesis, self-assembly, properties to applications. *Prog. Polym. Sci.* **2021**, *116*, 101387.

[93] Mei, G. H.; Zheng, Y. N.; Fu, Y. R.; Huo, M. Polymerization-induced self-assembly of random bottlebrush copolymers. *Polym. Chem.* **2022**, *13*, 5389–5396.

[94] Sun, Z. H.; Liu, R. Z.; Su, T. Y.; Huang, H. J.; Kawamoto, K.; Liang, R. Q.; Liu, B.; Zhong, M. J.; Alexander-Katz, A.; Ross, C. A. et al. Emergence of layered nanoscale mesh networks through intrinsic molecular confinement self-assembly. *Nat. Nanotechnol.* **2023**, *18*, 273–280.

[95] Jakobi, B.; Bichler, K. J.; Juranyi, F.; Schneider, G. J. Reversed dynamics of bottlebrush polymers with stiff backbone and flexible side chains. *J. Chem. Phys.* **2024**, *160*, 084901.

[96] Wilk, J. T.; Furner, C. T.; Kent, E. W.; Kelly, M. T.; Zhao, B.; Li, C. Y. Effect of grafting density on the crystallization behavior of molecular bottlebrushes. *Macromolecules* **2024**, *57*, 8487–8497.

[97] Hu, M. Q.; Seong, H. G.; Dimitriyev, M. S.; Hu, W. G.; Chen, Z.; Gan, X. C.; Grason, G. M.; Emrick, T.; Russell, T. P. Backbone stitching in bottlebrush copolymer mesodomains and the impact of side chain crystallization. *Macromolecules* **2025**, *58*, 1547–1561.

[98] Bichler, K. J.; Jakobi, B.; Sarter, M.; Schneider, G. J. Backbone dynamics of bottlebrush polymers studied by neutron scattering. *Macromolecules* **2025**, *58*, 11180–11191.

[99] Chen, Q. Y.; Tian, K.; Zhu, R. Q.; Ding, M. M.; Xu, Z. W. Self-assembly of amphiphilic comb-like copolymers into micelles and vesicles in solution. *Polymers* **2025**, *17*, 1870.

[100] Lotocki, V.; Battaglia, A. M.; Moon, N.; Titi, H. M.; Seferos, D. S. Conjugated core-shell bottlebrush polymers that exhibit crystallization-driven self-assembly. *Chem. Sci.* **2025**, *16*, 920–932.

[101] Sun, Z. H.; Liu, B.; Ma, M. C.; Alexander-Katz, A.; Ross, C. A.; Johnson, J. A. ROMP of macromonomers prepared by ROMP: Expanding access to complex, functional bottlebrush polymers. *J. Am. Chem. Soc.* **2025**, *147*, 3855–3865.

[102] Boott, C. E.; Gwyther, J.; Harniman, R. L.; Hayward, D. W.; Manners, I. Scalable and uniform 1D nanoparticles by synchronous polymerization, crystallization and self-assembly. *Nat. Chem.* **2017**, *9*, 785–792.

[103] Oliver, A. M.; Gwyther, J.; Boott, C. E.; Davis, S.; Pearce, S.; Manners, I. Scalable fiber-like micelles and block co-micelles by polymerization-induced crystallization-driven self-assembly. *J. Am. Chem. Soc.* **2018**, *140*, 18104–18114.

[104] Ellis, C. E.; Garcia-Hernandez, J. D.; Manners, I. Scalable and uniform length-tunable biodegradable block copolymer nanofibers with a polycarbonate core via living polymerization-induced crystallization-driven self-assembly. *J. Am. Chem. Soc.* **2022**, *144*, 20525–20538.

[105] Chen, S. L.; Wang, Y. M.; Dong, X. L.; Xing, M. X.; Mei, J. Q.; Qu, X. W.; Wang, F. F. Kinetic self-assembly of hierarchical V-notch spherulites via asynchronous polymerization-crystallization for multiscale anticounterfeiting. *J. Am. Chem. Soc.* **2026**, *148*, 10835–10847.

[106] Sangroniz, L.; Sangroniz, A.; Shi, C. X.; Scoti, M.; Ximenis, M.; De Rosa, C.; Chen, E. Y. X.; Sardon, H.; Müller, A. J. Tacticity-independent crystallization of polymers. *Nat. Chem.* **2026**, *18*, 625–638.

[107] Xu, J. J.; Ma, Y.; Hu, W. B.; Rehahn, M.; Reiter, G. Cloning polymer single crystals through self-seeding. *Nat. Mater.* **2009**, *8*, 348–353.

[108] Kaner, P.; Ruiz-Orta, C.; Boz, E.; Wagener, K. B.; Tasaki, M.; Tashiro, K.; Alamo, R. G. Kinetic control of chlorine packing in crystals of a precisely substituted polyethylene. Toward advanced polyolefin materials. *Macromolecules* **2014**, *47*, 236–245.

[109] Song, S. F.; Miao, W. J.; Wang, Z. B.; Gong, D. R.; Chen, Z. R. Synthesis and characterization of precisely-defined ethylene-co-aryl ether polymers via ADMET polymerization. *Polymer* **2015**, *64*, 76–83.

[110] Song, S. F.; Guo, Y. T.; Wang, R. Y.; Fu, Z. S.; Xu, J. T.; Fan, Z. Q. Synthesis and crystallization behavior of equisequential ADMET polyethylene containing arylene ether defects: Remarkable effects of substitution position and arylene size. *Macromolecules* **2016**, *49*, 6001–6011.

[111] Song, S. F.; He, F.; Fu, Z. S.; Xu, J. T.; Fan, Z. Q. Precision ADMET polyolefins containing dithiane: Synthesis, thermal properties, and macromolecular transformation. *J. Polym. Sci. Part A: Polym. Chem.* **2016**, *54*, 2468–2475.

[112] Song, S. F.; Guo, W. Q.; Zou, S. F.; Fu, Z. S.; Xu, J. T.; Fan, Z. Q. Polyethylene containing aliphatic ring and aromatic ring defects in the main chain: Synthesis via ADMET and comparisons of thermal properties and crystalline structure. *Polymer* **2016**, *107*, 113–121.

[113] Zhang, X. S.; Zhang, W.; Wagener, K. B.; Boz, E.; Alamo, R. G. Effect of self-poisoning on crystallization kinetics of dimorphic precision polyethylenes with bromine. *Macromolecules* **2018**, *51*, 1386–1397.

[114] He, X. M.; Hsiao, M. S.; Boott, C. E.; Harniman, R. L.; Nazemi, A.; Li, X. Y.; Winnik, M. A.; Manners, I. Two-dimensional assemblies from crystallizable homopolymers with charged termini. *Nat. Mater.* **2017**, *16*, 481–488.

[115] Song, S. F.; Zhou, H.; Ye, S. Y.; Tam, J.; Howe, J. Y.; Manners, I.; Winnik, M. A. Spherulite-like micelles. *Angew. Chem., Int. Ed.* **2021**, *60*, 10950–10956.

[116] Jiang, J. J.; Winnik, M. A. Three-dimensional polymer micelles formed by crystallization-driven self-assembly. *Acc. Chem. Res.* **2025**, *58*, 1683–1695.

[117] Qiu, H. B.; Gao, Y.; Du, V. A.; Harniman, R.; Winnik, M. A.; Manners, I. Branched micelles by living crystallization-driven block copolymer self-assembly under kinetic control. *J. Am. Chem. Soc.* **2015**, *137*, 2375–2385.

[118] Gilroy, J. B.; Gädt, T.; Whittell, G. R.; Chabanne, L.; Mitchels, J. M.; Richardson, R. M.; Winnik, M. A.; Manners, I. Monodisperse cylindrical micelles by crystallization-driven living self-assembly. *Nat. Chem.* **2010**, *2*, 566–570.

[119] Tao, D. L.; Feng, C.; Cui, Y. N.; Yang, X.; Manners, I.; Winnik, M. A.; Huang, X. Y. Monodisperse fiber-like micelles of controlled length and composition with an oligo(p-phenylenevinylene) core via "living" crystallization-driven self-assembly. *J. Am. Chem. Soc.* **2017**, *139*, 7136–7139.

[120] Qiu, H. B.; Gao, Y.; Boott, C. E.; Gould, O. E. C.; Harniman, R. L.; Miles, M. J.; Webb, S. E. D.; Winnik, M. A.; Manners, I. Uniform patchy and hollow rectangular platelet micelles from crystallizable polymer blends. *Science* **2016**, *352*, 697–701.

[121] Xu, J. P.; Zhou, H.; Yu, Q.; Guerin, G.; Manners, I.; Winnik, M. A. Synergistic self-seeding in one-dimension: A route to patchy and block comicelles with uniform and controllable length. *Chem. Sci.* **2019**, *10*, 2280–2284.

[122] Song, S. F.; Jiang, J. J.; Nikbin, E.; Howe, J. Y.; Manners, I.; Winnik, M. A. The role of cooling rate in crystallization-driven block copolymer self-assembly. *Chem. Sci.* **2022**, *13*, 396–409.

[123] Fang, E.; Li, R. Y.; Chen, S.; Wang, Z. H.; Song, S. F.; Li, H. Y. Establishing precise relationship between pendant length and tunable thickness of nanocrystals formed by polymers with crystalline linear alkyl side chains. *Macromolecules* **2026**, *59*, 6443–6454.

[124] Gädt, T.; Ieong, N. S.; Cambridge, G.; Winnik, M. A.; Manners, I. Complex and hierarchical micelle architectures from diblock copolymers using living, crystallization-driven polymerizations. *Nat. Mater.* **2009**, *8*, 144–150.

[125] Qiu, H. B.; Cambridge, G.; Winnik, M. A.; Manners, I. Multi-armed micelles and block co-micelles via crystallization-driven self-assembly with homopolymer nanocrystals as initiators. *J. Am. Chem. Soc.* **2013**, *135*, 12180–12183.

[126] Li, X. Y.; Gao, Y.; Boott, C. E.; Winnik, M. A.; Manners, I. Non-covalent synthesis of supermicelles with complex architectures using spatially confined hydrogen-bonding interactions. *Nat. Commun.* **2015**, *6*, 8127.

[127] Qiu, H. B.; Hudson, Z. M.; Winnik, M. A.; Manners, I. Multidimensional hierarchical self-assembly of amphiphilic cylindrical block comicelles. *Science* **2015**, *347*, 1329–1332.

[128] Li, X. Y.; Gao, Y.; Boott, C. E.; Hayward, D. W.; Harniman, R.; Whittell, G. R.; Richardson, R. M.; Winnik, M. A.; Manners, I. "Cross" supermicelles via the hierarchical assembly of amphiphilic cylindrical triblock comicelles. *J. Am. Chem. Soc.* **2016**, *138*, 4087–4095.

[129] Li, X. Y.; Gao, Y.; Harniman, R.; Winnik, M.; Manners, I. Hierarchical assembly of cylindrical block comicelles mediated by spatially confined hydrogen-bonding interactions. *J. Am. Chem. Soc.* **2016**, *138*, 12902–12912.

[130] Zhu, Y. L.; Han, L.; Fan, H.; Wang, M. J.; Qi, R.; Zhao, Y.; He, F. Three-dimensional spirals of conjugated block copolymers driven by screw dislocation. *Macromolecules* **2020**, *53*, 3217–3223.

[131] Zhang, Y. F.; Pearce, S.; Eloi, J. C.; Harniman, R. L.; Tian, J.; Cordoba, C.; Kang, Y. T.; Fukui, T.; Qiu, H. B.; Blackburn, A. et al. Dendritic micelles with controlled branching and sensor applications. *J. Am. Chem. Soc.* **2021**, *143*, 5805–5814.

[132] Jia, L.; Guerin, G.; Lu, Y. J.; Yu, Q.; Manners, I.; Winnik, M. A. Creating biomorphic barbed and branched mesostructures in solution through block copolymer crystallization. *Angew. Chem., Int. Ed.* **2018**, *57*, 17205–17210.

[133] He, F.; Gädt, T.; Jones, M.; Scholes, G. D.; Manners, I.; Winnik, M. A. Synthesis and self-assembly of fluorescent micelles from poly(ferrocenyldimethylsilane-*b*-2-vinylpyridine-*b*-2, 5-di(2′-ethylhexyloxy)-1, 4-phenylvinylene) triblock copolymer. *Macromolecules* **2009**, *42*, 7953–7960.

[134] Chen, W. Y.; Li, C. Y.; Zheng, J. X.; Huang, P.; Zhu, L.; Ge, Q.; Quirk, R. P.; Lotz, B.; Deng, L. F.; Wu, C. et al. "Chemically shielded" poly(ethylene oxide) single crystal growth and construction of channel-wire arrays with chemical and geometric recognitions on a submicrometer scale. *Macromolecules* **2004**, *37*, 5292–5299.

[135] Wang, Z. W.; Qiu, J. J.; Wang, X. S.; Zhang, Z. P.; Chen, Y. H.; Huang, X.; Huang, W. Two-dimensional light-emitting materials: Preparation, properties and applications. *Chem. Soc. Rev.* **2018**, *47*, 6128–6174.

[136] Zhang, S.; Chen, R. Z.; Kong, D. R.; Chen, Y. H.; Liu, W. T.; Jiang, D. D.; Zhao, W. Y.; Chang, C.; Yang, Y. G.; Liu, Y. Q. et al. Photovoltaic nanocells for high-performance large-scale-integrated organic phototransistors. *Nat. Nanotechnol.* **2024**, *19*, 1323–1332.

[137] Yang, Y.; Knapp, A.; Bodesheim, D.; Croy, A.; Hambsch, M.; Hermes, I.; Naisa, C.; Pohl, D.; Rellinghaus, B.; Zhao, C. S. et al. Mechanically interlocked monolayer and bilayer two-dimensional polymers with high elastic modulus. *Nat. Synth.* **2026**, *5*, 357–366.

[138] Chen, L. Y.; Wang, Z. H.; Fang, E.; Guo, Y. H.; Liu, Z. M.; Song, W.; Li, H. Y.; Xu, J. T.; Fan, Z. Q.; Winnik, M. A. et al. Recyclable polypentenamers with precise crystallization and versatile functionalization. *Macromolecules* **2025**, *58*, 1048–1059.

[139] Wang, Z. H.; Fang, E.; Chen, L. Y.; Guo, Y. H.; Fan, Z. Q.; Song, S. F. Recyclable biomass-derived polyethylene-like plastics. *Macromolecules* **2025**, *58*, 9712–9723.

[140] Wang, Z. H.; Fang, E.; Chen, L. Y.; He, Z. J.; Xu, J. T.; Winnik, M. A.; Song, S. F. Programming crystal thickness by precision chain folding in architecturally designed polymers. *J. Am. Chem. Soc.* **2026**, *148*, 14096–14106.

[141] Guan, S.; Deng, Z. C.; Huang, T. Y.; Wen, W.; Zhao, Y. B.; Chen, A. H. Light-triggered reversible slimming of azobenzene-containing wormlike nanoparticles synthesized by polymerization-induced self-assembly for nanofiltration switches. *ACS Macro Lett.* **2019**, *8*, 460–465.

[142] Yang, S.; Shin, S.; Choi, I.; Lee, J.; Choi, T. L. Direct formation of large-area 2D nanosheets from fluorescent semiconducting homopolymer with orthorhombic crystalline orientation. *J. Am. Chem. Soc.* **2017**, *139*, 3082–3088.

[143] Xia, T. L.; Tong, Z. Z.; Xie, Y. J.; Arno, M. C.; Lei, S. X.; Xiao, L. H.; Rho, J. Y.; Ferguson, C. T. J.; Manners, I.; Dove, A. P. et al. Tuning the functionality of self-assembled 2D platelets in the third dimension. *J. Am. Chem. Soc.* **2023**, *145*, 25274–25282.

[144] Hils, C.; Schmelz, J.; Drechsler, M.; Schmalz, H. Janus micelles by crystallization-driven self-assembly of an amphiphilic, double-crystalline triblock terpolymer. *J. Am. Chem. Soc.* **2021**, *143*, 15582–15586.

[145] Zhang, C. X.; Pan, H.; Zhou, Y. F. Chain-folding of alternating copolymers to achieve main-chain alkyl chain crystallization with minimum six carbon atoms. *Macromolecules* **2023**, *56*, 7870–7878.

[146] Xu, J.; Wu, H. C.; Wang, J.; Xu, L.; Zhang, G.; Wang, C.; Wang, Z.; Han, Y.; Zhang, X. Tuning the layer thickness of poly(ethylene oxide) 2D platelets by controlled chain folding. *Nano Letters* **2024**, *24*, 4717–4724.

[147] Gao, Z. Q.; Zhang, X.; Zheng, B. W.; Gu, J. Y.; Tong, Z. Z. Creation of segmented platelets with diverse crystalline cores using double crystalline triblock copolymers. *J. Am. Chem. Soc.* **2025**, *147*, 5172–5181.

[148] Song, S. F.; Xing, Z. Y.; Cheng, Z. M.; Fu, Z. S.; Xu, J. T.; Fan, Z. Q. Functional polyethylene with regularly distributed ester pendants via ring-opening metathesis polymerization of ester functionalized cyclopentene: Synthesis and characterization. *Polymer* **2017**, *129*, 135–143.

[149] Song, S. F.; Zhang, Z.; Liu, X. Y.; Fu, Z. S.; Xu, J. T.; Fan, Z. Q. Synthesis and characterization of functional polyethylene with regularly distributed thioester pendants via ring-opening metathesis polymerization. *J. Polym. Sci. Part A: Polym. Chem.* **2017**, *55*, 4027–4036.

[150] Keller, A. A note on single crystals in polymers: Evidence for a folded chain configuration. *Philos. Mag.* **1957**, *2*, 1171–1175.

[151] Fischer, E. W. Notizen: Stufen- und spiralförmiges kristallwachstum bei hochpolymeren. *Z. Naturforsch. A* **1957**, *12*, 753–754.

[152] Till, P. H. Jr. The growth of single crystals of linear polyethylene. *J. Polym. Sci.* **1957**, *24*, 301–306.

[153] Brisson, E. R. L.; Worthington, M. J. H.; Kerai, S.; Müllner, M. Nanoscale polymer discs, toroids and platelets: A survey of their syntheses and potential applications. *Chem. Soc. Rev.* **2024**, *53*, 1984–2021.

[154] Champion, J. A.; Katare, Y. K.; Mitragotri, S. Particle shape: A new design parameter for micro- and nanoscale drug delivery carriers. *J. Controlled Release* **2007**, *121*, 3–9.

[155] Gratton, S. E. A.; Ropp, P. A.; Pohlhaus, P. D.; Luft, J. C.; Madden, V. J.; Napier, M. E.; DeSimone, J. M. The effect of particle design on cellular internalization pathways. *Proc. Natl. Acad. Sci. USA* **2008**, *105*, 11613–11618.

[156] Decuzzi, P.; Godin, B.; Tanaka, T.; Lee, S. Y.; Chiappini, C.; Liu, X.; Ferrari, M. Size and shape effects in the biodistribution of intravascularly injected particles. *J. Controlled Release* **2010**, *141*, 320–327.

[157] Cabral, H.; Matsumoto, Y.; Mizuno, K.; Chen, Q.; Murakami, M.; Kimura, M.; Terada, Y.; Kano, M. R.; Miyazono, K.; Uesaka, M. et al. Accumulation of sub-100 nm polymeric micelles in poorly permeable tumours depends on size. *Nat. Nanotechnol.* **2011**, *6*, 815–823.